J|A|C|S ARTICLES

Published on Web 01/12/2009

Probing Heteronuclear $^{15}N-^{17}O$ and $^{13}C-^{17}O$ Connectivities and Proximities by Solid-State NMR Spectroscopy

Ivan Hung,[†,⊥] Anne-Christine Uldry,[‡,#] Johanna Becker-Baldus,[†] Amy L. Webber,[†] Alan Wong,[†,▽] Mark E. Smith,[†] Siân A. Joyce,[§] Jonathan R. Yates,[||] Chris J. Pickard,[‡] Ray Dupree,[†] and Steven P. Brown*[,†]

Department of Physics, University of Warwick, Coventry CV4 7AL, U.K., School of Physics and Astronomy, University of St. Andrews, North Haugh, St. Andrews KY16 9SS, U.K., Tyndall National Institute, Lee Maltings, Prospect Row, Cork, Ireland, and TCM Group, Cavendish Laboratory, University of Cambridge, 19 J. J. Thomson Avenue, Cambridge CB3 OHE, U.K.

Received July 28, 2008; E-mail: S.P.Brown@warwick.ac.uk

Abstract: Heteronuclear solid-state magic-angle spinning (MAS) NMR experiments for probing $^{15}N-^{17}O$ dipolar and *J* couplings are presented for [$^{2}H(NH_3)$,1-^{13}C,^{15}N,$^{17}O_2$]glycine·^{2}HCl and [$^{15}N_2$,$^{17}O_2$]uracil. Two-dimensional $^{15}N-^{17}O$ correlation spectra are obtained using the R^3-HMQC experiment; for glycine·^{2}HCl, the intensity of the resolved peaks for the C=O and C−O^{2}H ^{17}O resonances corresponds to the relative magnitude of the respective $^{15}N-^{17}O$ dipolar couplings. $^{17}O-^{15}N$ REDOR curves are presented for glycine·^{2}HCl; fits of the initial buildup ($\Delta S/S < 0.2$) yield effective dipolar couplings in agreement with (±20%) the root-sum-squared dipolar couplings determined from the crystal structure. Experimental $^{15}N-^{17}O$ REAPDOR curves for the ^{15}N resonances in glycine·^{2}HCl and uracil fit well to the universal curve presented by Goldbourt et al. (*J. Am. Chem. Soc.* **2003**, *125*, 11194). Heteronuclear $^{13}C-^{17}O$ and $^{15}N-^{17}O$ *J* couplings were experimentally determined from fits of the quotient of the integrated intensity obtained in a heteronuclear and a homonuclear spin−echo experiment, $S_Q(\tau) = S_{HET}(\tau)/S_{HOM}(\tau)$. For glycine·^{2}HCl, $^{1}J_{CO}$ was determined as 24.7 ± 0.2 and 25.3 ± 0.3 Hz for the C=O and C−O^{2}H resonances, respectively, while for uracil, the average of the two NH···O hydrogen-bond-mediated *J* couplings was determined as 5.1 ± 0.6 Hz. In addition, two-bond intramolecular *J* couplings, $^{2}J_{OO} = 8.8 \pm 0.9$ Hz and $^{2}J_{N1,N3} = 2.7 \pm 0.1$ Hz, were determined for glycine·^{2}HCl and uracil, respectively. Excellent agreement was found with *J* couplings calculated using the CASTEP code using geometrically optimized crystal structures for glycine·HCl [$^{1}J_{CO}$(C=O) = 24.9 Hz, $^{1}J_{CO}$(C−OH) = 27.5 Hz, $^{2}J_{OO} = 7.9$ Hz] and uracil [$^{2h}J_{N1,O4} = 6.1$ Hz, $^{2h}J_{N3,O4} = 4.6$ Hz, $^{2}J_{N1,N3} = 2.7$ Hz].

1. Introduction

The structural and dynamic information inherent to through-space dipolar and through-bond *J* couplings is a key reason why NMR has become such an indispensable analytical tool. Of the elements most commonly found in organic and biological solids (i.e., hydrogen, carbon, nitrogen, and oxygen), heteronuclear solid-state NMR experiments involving the spin $I = 1/2$ isotopes of hydrogen, carbon, and nitrogen are commonly employed (^{1}H, ^{13}C, and ^{15}N).[1−4] The only NMR-active isotope of oxygen is the $I = 5/2$ ^{17}O nucleus, which has a low sensitivity due to its very low natural abundance (0.037%) and low resonance frequency ($\gamma = -3.628 \times 10^7$ rad T^{-1} s^{-1}), as well as the presence of an electric quadrupole moment ($Q = -2.6 \times 10^{-30}$ m^2). With isotopic enrichment, ^{17}O NMR is being increasingly used in the study of inorganic materials,[5] as well as organic and biological molecules.[6] However, relatively few heteronuclear experiments involving oxygen have been presented. Cross polarization (CP) from ^{1}H or ^{27}Al to ^{17}O has been demonstrated,[7−11] while ^{17}O/^{1}H REDOR has been employed to investigate $^{17}O-^{1}H$ proximities in zeolites HY and HZSM-5.[12] $^{13}C-^{17}O$ distance measurements via the SEDOR, REDOR, and REAPDOR techniques have also been reported for CO

[†] University of Warwick.
[‡] University of St. Andrews.
[§] Tyndall National Institute.
[||] University of Cambridge.
[⊥] Current address: NHMFL, 1800 East Paul Dirac Drive, Tallahassee, Florida 32310.
[#] Current address: Paul Scherrer Institute, 5232 Villigen PSI, Switzerland.
[▽] Current address: CEA Saclay, SCM, Gif-sur-Yvette 91191, France.

(1) Goldbourt, A.; Gross, B. J.; Day, L. A.; McDermott, A. E. *J. Am. Chem. Soc.* **2007**, *129*, 2338.
(2) Chevelkov, V.; Faelber, K.; Schrey, A.; Rehbein, K.; Diehl, A.; Reif, B. *J. Am. Chem. Soc.* **2007**, *129*, 10195.
(3) Pintacuda, G.; Giraud, N.; Pierattelli, R.; Bockmann, A.; Bertini, I.; Emsley, L. *Angew. Chem., Int. Ed. Engl.* **2007**, *46*, 1079.
(4) Andronesi, O. C.; von Bergen, M.; Biernat, J.; Seidel, K.; Griesinger, C.; Mandelkow, E.; Baldus, M. *J. Am. Chem. Soc.* **2008**, *130*, 5922.
(5) Ashbrook, S. E.; Smith, M. E. *Chem. Soc. Rev.* **2006**, *35*, 718.
(6) Wu, G. *Prog. Nucl. Magn. Reson. Spectrosc.* **2008**, *52*, 118.
(7) Walter, T. H.; Turner, G. L.; Oldfield, E. *J. Magn. Reson.* **1988**, *76*, 106.
(8) Gann, S. L.; Baltisberger, J. H.; Wooten, E. W.; Zimmermann, H.; Pines, A. *Bull. Magn. Reson.* **1994**, *16*, 68.
(9) Kuroki, S.; Takahashi, A.; Ando, I.; Shoji, A.; Ozaki, T. *J. Mol. Struct.* **1994**, *323*, 197.
(10) Ashbrook, S. E.; Wimperis, S. *J. Magn. Reson.* **2000**, *147*, 238.
(11) Ashbrook, S. E.; Wimperis, S. *Mol. Phys.* **2000**, *98*, 1.
(12) Peng, L.; Huo, H.; Liu, Y.; Grey, C. P. *J. Am. Chem. Soc.* **2007**, *129*, 335.

10.1021/ja805898d CCC: $40.75

chemisorbed on Pd metal,[13] L-tyrosine,[14] and asparagine monohydrate,[15] as well as the differentiation of parallel and antiparallel β-sheets formed by L-alanyl-alanyl-alanine.[16] Recently, experiments incorporating the symmetry-based recoupling of $^1H-^{17}O$ heteronuclear dipolar couplings have been presented, namely modified REDOR experiments that enable the measurement of intra- and intermolecular $^1H-^{17}O$ distances in L-tyrosine·HCl[17,18] and $^1H\rightarrow^{17}O$ polarization transfer using the PRESTO-II sequence applied to glycine·HCl and $Mg(OH)_2$.[19] Furthermore, the mobility of ^{17}O nuclei and the assignment of ^{17}O and ^{51}V sites in anionic conductive materials (α-$Bi_4V_2O_{11}$ and γ-$Bi_4V_{1.7}Ti_{0.3}O_{10.85}$) using $^{17}O/^{51}V$ TRAPDOR experiments has been reported.[20] A few instances of two-dimensional (2D) heteronuclear experiments can also be found in the literature. In particular, 2D experiments devised to examine the relative orientation between the ^{17}O quadrupole tensors and the O−H dipole tensors in glycine·HCl,[19] $Mg(OH)_2$,[19,21] and $Mg(OH)_x(OCH_3)_{2-x}$[21] have been reported. Recently, through-bond $^{27}Al/^{17}O$ 2D HMQC correlation spectra for crystalline $CA2(CaAl_2O_7)$ and vitreous $CA(CaO-Al_2O_3)$ have also been presented.[22] From the scarcity of ^{17}O heteronuclear studies in the literature, it can be seen that considerable scope remains for further development of solid-state NMR experiments that probe proximities and connectivity with ^{17}O nuclei, leading to additional constraints for structural elucidation.

Despite the importance of NH···O hydrogen bonds in organic and biological solids, to the best of our knowledge, $^{15}N-^{17}O$ solid-state NMR experiments have not previously been presented, with their proximate Larmor frequencies and combined low sensitivity representing difficult hurdles to overcome. In this paper, we demonstrate the feasibility of solid-state NMR experiments that utilize and probe $^{15}N-^{17}O$ dipolar and J couplings for two model compounds, glycine·^{2}HCl and uracil.

2. Experimental and Computational Details

2.1. Materials and Synthesis. The sample of [$^2H(NH_3)$,1-^{13}C,^{15}N,$^{17}O_2$]glycine·^{2}HCl was prepared as described previously[23] by using commercially available [1-^{13}C,^{15}N]glycine (Sigma-Aldrich, UK) and [70%-^{17}O]H_2O (CortecNet, France) as starting materials, with subsequent deuteration of the exchangeable protons (COOH, NH_3) being achieved by recrystallization from D_2O. [1,3-^{15}N]Uracil (Sigma-Aldrich, UK) was enriched with [70%-^{17}O]H_2O according to the literature protocol, resulting in [1,3-^{15}N,2,4-^{17}O]uracil.[24,25]

2.2. Solid-State NMR. All experiments were performed on a Bruker AVANCE II+ NMR spectrometer, operating at ^1H, ^{13}C, ^{15}N, and ^{17}O Larmor frequencies of 600, 151, 61, and 81 MHz, respectively, using a Bruker 3.2 mm triple-resonance magic-angle spinning (MAS) probe. Unless otherwise stated, ^{13}C and ^{15}N $\pi/2$ pulses of 5.0 μs, corresponding to a nutation frequency (ν_1) equal to 50 kHz, were used, while "central-transition-selective" $\pi/2$ pulses of 5.0 μs were used for ^{17}O, corresponding to $\nu_1 = 16.7$ kHz (i.e., taking into account the scaling by $(I + 1/2)^{-1}$). SPINAL-64 heteronuclear decoupling[26] was used with $\nu_1(^1H) = 100$ kHz. Ramped cross polarization[27] was employed for the acquisition of all ^{13}C and ^{15}N spectra with a contact time of 1.0 ms, a ^1H $\pi/2$-pulse duration of 2.5 μs, and (except where otherwise stated) a recycle delay of 4.0 s. For ^{17}O experiments (except where otherwise stated), recycle delays of 0.5 s (glycine·^{2}HCl) and 1.0 s (uracil) were used. RAPT[28] ($n = 3$, $\nu_{off} = 450$ kHz) was used for signal enhancement in ^{17}O 1D experiments.

^{15}N chemical shifts were referenced indirectly to neat liquid nitromethane (CH_3NO_2) by using powdered [^{15}N]glycine as an external secondary reference ($\delta_{iso} = -347.4$ ppm). To convert to the chemical shift scale frequently used in protein NMR, where the reference is liquid ammonia at −50 °C, it is necessary to add 379.5 ppm to the given values. The ^{13}C chemical shifts were referenced to tetramethylsilane (TMS, $Si(CH_3)_4$) by using powdered l-[1-^{13}C]alanine as an external secondary reference ($\delta_{iso} = 177.9$ ppm). The ^{17}O chemical shift scale was referenced to the ^{17}O signal of H_2O set to 0.0 ppm.

2D $^{17}O/^{15}N$ R^3-HMQC NMR spectra were acquired with the pulse sequence shown in Figure 1a, related versions of which have been used previously to record $^1H/^{14}N$, $^1H/^{27}Al$, and $^{23}Na/^{31}P$ correlation spectra.[29,30] A 16-step phase cycle was used, $\varphi_1 = +x, -x$; $\varphi_2 = +x, +x, +x, +x, +y, +y, +y, +y, -x, -x, -x, -x, -y, -y, -y, -y$; $\varphi_3 = +y, +y, -y, -y$; $\varphi_4 = -y$; receiver $= -x, +x, +x, -x, +x, -x, -x, +x, -x, +x, +x, -x, +x, -x, -x, +x$, to select $\Delta p = \pm 1$ on the ^{17}O $\pi/2$ pulse (φ_1), $\Delta p = \pm 2$ on the ^{17}O π pulse (φ_2), and $\Delta p = \pm 1$ on the first ^{15}N $\pi/2$ pulse (φ_3), where p is the coherence order. Sign discrimination in F_1 was achieved using the States hyper-complex processing method.[31] A total of 512 (glycine·^{2}HCl) or 1024 (uracil) transients were coadded for each of 206 (glycine·^{2}HCl) or 130 (uracil) t_1 slices, resulting in a total experimental time of 14.6 h (glycine·^{2}HCl) or 18.5 h (uracil). Spectral widths of 50.0 and 11.75 kHz (glycine·^{2}HCl) or 80.0 and 5.0 kHz (uracil) were employed along the F_2 and F_1 dimensions, respectively. The ^{15}N carrier frequency was set at −299.1 (glycine·^{2}HCl) and −237.5 (uracil) ppm. R^3 dipolar recoupling was achieved by applying pulses for $\tau/2 = 280\tau_r \approx 11.9$ ms at $\nu_1 = \nu_r = 23.5$ kHz (glycine·^{2}HCl) or $\tau/2 = 160\tau_r \approx 8.0$ ms at $\nu_1 = \nu_r = 20.0$ kHz (uracil), where ν_r and τ_r denote the MAS frequency and the rotor period, respectively.

$^{17}O/^{15}N$ REDOR spectra of glycine·^{2}HCl were acquired at 22.5 kHz MAS, with a recycle delay of 2 s. The REDOR pulse sequence as employed previously for $^{23}Na/^{31}P$ and $^{27}Al/^{31}P$ REDOR experiments[32] is shown in Figure 1b. The REDOR fraction ($\Delta S/S = (S - S_r)/S$) was determined from spectra acquired without (S_r) and with (S) the central ^{15}N pulse, where the r subscript refers to the reduced signal intensity in the dephased (under the heteronuclear

(13) Shore, S. E.; Ansermet, J. P.; Slichter, C. P.; Sinfelt, J. H. *Phys. Rev. Lett.* **1987**, *58*, 953.
(14) Gullion, T. *J. Magn. Reson. Ser. A* **1995**, *117*, 326.
(15) Chopin, L.; Vega, S.; Gullion, T. *J. Am. Chem. Soc.* **1998**, *120*, 4406.
(16) Gullion, T.; Yamauchi, K.; Okonogi, M.; Asakura, T. *Macromolecules* **2007**, *40*, 1363.
(17) Brinkmann, A.; Kentgens, A. P. M. *J. Am. Chem. Soc.* **2006**, *128*, 14758.
(18) Brinkmann, A.; Kentgens, A. P. M. *J. Phys. Chem. B* **2006**, *110*, 16089.
(19) van Beek, J. D.; Dupree, R.; Levitt, M. H. *J. Magn. Reson.* **2006**, *179*, 38.
(20) Kim, N.; Grey, C. P. *Science* **2002**, *297*, 1317.
(21) van Eck, E. R. H.; Smith, M. E. *J. Chem. Phys.* **1998**, *108*, 5904.
(22) Iuga, D.; Morais, C.; Gan, Z. H.; Neuville, D. R.; Cormier, L.; Massiot, D. *J. Am. Chem. Soc.* **2005**, *127*, 11540.
(23) Wong, A.; Hung, I.; Howes, A. P.; Anupold, T.; Past, J.; Samoson, A.; Brown, S. P.; Smith, M. E.; Dupree, R. *Magn. Reson. Chem.* **2007**, *45*, S68.
(24) Wu, G.; Dong, S.; Ida, R.; Reen, N. *J. Am. Chem. Soc.* **2002**, *124*, 1768.
(25) Wu, G.; Dong, S. *J. Am. Chem. Soc.* **2001**, *123*, 9119.
(26) Fung, B. M.; Khitrin, A. K.; Ermolaev, K. *J. Magn. Reson.* **2000**, *142*, 97.
(27) Metz, G.; Wu, X. L.; Smith, S. O. *J. Magn. Reson. Ser. A* **1994**, *110*, 219.
(28) Kwak, H. T.; Prasad, S.; Clark, T.; Grandinetti, P. J. *J. Magn. Reson.* **2003**, *160*, 107.
(29) Gan, Z. H.; Amoureux, J. P.; Trebosc, J. *Chem. Phys. Lett.* **2007**, *435*, 163.
(30) Trebosc, J.; Hu, B.; Amoureux, J. P.; Gan, Z. *J. Magn. Reson.* **2007**, *186*, 220.
(31) States, D. J.; Haberkorn, R. A.; Ruben, D. J. *J. Magn. Reson.* **1982**, *48*, 286.
(32) Chan, J. C. C.; Eckert, H. *J. Magn. Reson.* **2000**, *147*, 170.
(33) Gullion, T. *Chem. Phys. Lett.* **1995**, *246*, 325.
(34) Goldbourt, A.; Vega, S.; Gullion, T.; Vega, A. J. *J. Am. Chem. Soc.* **2003**, *125*, 11194.

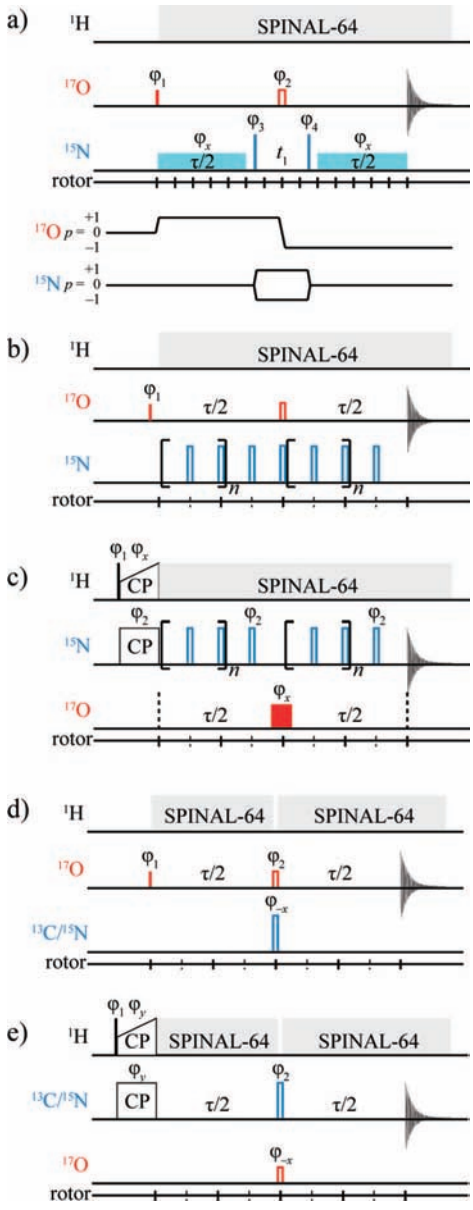

Figure 1. Pulse sequences for the (a) R^3-HMQC, (b) REDOR, (c) CP/REAPDOR, and heteronuclear spin−echo experiments with (d) one pulse and (e) CP excitation of the observed nucleus. The coherence transfer pathway diagram for (a) is shown below the pulse sequence. For the (b) REDOR and (c) CP/REAPDOR experiments, the reduced-intensity dephased (S_r) and reference (S) spectra correspond to experiments (b) without (S_r) and with (S) the central ^{15}N pulse and (c) with (S_r) and without (S) the ^{17}O pulse.

dipolar coupling) spectrum. A two-step phase cycle was used, $\varphi_1 = +x,-x$; receiver $= +x,-x$. The ^{15}N and ^{17}O π pulses were of duration 8 μs, while the initial ^{17}O direct excitation pulse was of duration 4 μs. A total of 1152 transients were coadded for the S_r and S experiments recorded for each τ duration.

^{15}N/^{17}O CP/REAPDOR spectra were acquired at various MAS frequencies observing on the ^{15}N channel and using pulses of duration one-third of a rotor period, $\tau_r/3$, on the ^{17}O channel with $\nu_1(^{17}O)$ approximately equal to 75 kHz. The REAPDOR fraction ($\Delta S/S = (S - S_r)/S$) was determined from spectra acquired with (S_r) and without (S) the ^{17}O adiabatic pulse. The REAPDOR pulse sequence, as previously used for X/Y experiments,[14−16,33−35] is shown in Figure 1c and employs an eight-step phase cycle, $\varphi_1 = +y, -y$; $\varphi_2 = +x, +x, -x, -x, +y, +y, -y, -y$; receiver $= +x, -x, -x, +x, +y, -y, -y, +y$, that selects $\Delta p = \pm 1$ on the ^{1}H $\pi/2$ pulse (φ_1) and $\Delta p = -1$ on the ^{15}N pulses (φ_2). Eight transients were coadded for the S_r and S experiments recorded for each τ duration. In both REDOR and REAPDOR experiments, the S_r and S spectra were recorded consecutively for each evolution interval, and the rotor-synchronized π-pulses on ^{15}N followed the XY-8 ($+x, +y, +x, +y, +y, +x, +y, +x$) phase alternation scheme.[36]

A ^{17}O/^{13}C and a ^{17}O/^{15}N heteronuclear spin−echo experiment was performed on glycine·^{2}HCl and uracil, respectively, using the pulse sequence shown in Figure 1d; such a pulse sequence has been used previously to determine ^{27}Al−^{31}P[37,38] and ^{71}Ga−^{31}P[39] J couplings. ^{17}O homonuclear spin−echo experiments were performed by omitting the π pulse on the nonobserved (i.e., ^{13}C or ^{15}N) channel. An eight-step phase cycle was used, $\varphi_1 = -x, +x$; $\varphi_2 = +y, +y, -x, -x, -y, -y, +x, +x$; receiver $= +x, -x, -x, +x, +x, -x, -x, +x$, to select $\Delta p = \pm 1$ and ± 2 on the ^{17}O $\pi/2$ (φ_1) and π pulses (φ_2), respectively. In total, 128 (6 s recycle delay) and 1152 (7.5 s recycle delay) transients were coadded for each τ increment for glycine·^{2}HCl and uracil, respectively.

A ^{13}C/^{17}O and a ^{15}N/^{17}O heteronuclear spin−echo experiment was performed on glycine·^{2}HCl and uracil, respectively, using the pulse sequence depicted in Figure 1e employing the same phase cycling as described above for the ^{17}O/^{13}C or ^{17}O/^{15}N experiment in Figure 1d. ^{13}C or ^{15}N homonuclear spin−echo experiments were performed by omitting the π pulse on the nonobserve (i.e., ^{17}O) channel. In total, 32 (6 s recycle delay) and 256 (7.5 s recycle delay) transients were coadded for each τ increment for the ^{13}C/^{17}O glycine·^{2}HCl and ^{15}N/^{17}O uracil experiments, respectively.

Where data corresponding to the quotient $S_Q(\tau) = S_{HET}(\tau)/S_{HOM}(\tau)$ are presented, the homonuclear and heteronuclear spin−echo spectra were recorded consecutively for each evolution interval. $S_{HET}(\tau)$ and $S_{HOM}(\tau)$ integrals were taken over the respective resolved peaks after Fourier transformation with respect to t_2. Errors on fitted parameters were determined using the covariance method as described in ref 40.

2.3. Computational Details. First-principles calculations were performed using the CASTEP[41] software package, which implements density functional theory using a plane-wave basis set and the pseudopotential approach and is thus applicable to periodic systems.

Starting with the crystal structures of glycine·HCl[42] and uracil[43] (CSD reference codes GLYHCL01 and URACIL), geometry optimizations (at fixed lattice parameters) were performed. For glycine·HCl, the Trouiller−Martins norm-conserving pseudopotentials[44] with a plane-wave cutoff at 1200 eV and a k-point density of 0.07 Å^{-1} were used. For a first optimization where only the hydrogen atoms were relaxed, high forces (up to 4.2 eV/Å) remained, such that a full relaxation of all atoms was performed. The geometry optimization of the uracil crystal structure has been described in ref 45, where all the atoms in the unit cell were relaxed.

(35) Gullion, T.; Vega, A. J. *Prog. Nucl. Magn. Reson. Spectrosc.* **2005**, *47*, 123.
(36) Gullion, T.; Baker, D. B.; Conradi, M. S. *J. Magn. Reson.* **1990**, *89*, 479.
(37) Amoureux, J. P.; Trebosc, J.; Wiench, J. W.; Massiot, D.; Pruski, M. *Solid State Nucl. Magn. Reson.* **2005**, *27*, 228.
(38) Massiot, D.; Fayon, F.; Alonso, B.; Trebosc, J.; Amoureux, J. P. *J. Magn. Reson.* **2003**, *164*, 160.
(39) Montouillout, V.; Morais, C. M.; Douy, A.; Fayon, F.; Massiot, D. *Magn. Reson. Chem.* **2006**, *44*, 770.
(40) Pham, T. N.; Griffin, J. M.; Masiero, S.; Lena, S.; Gottarelli, G.; Hodgkinson, P.; Fillip, C.; Brown, S. P. *Phys. Chem. Chem. Phys.* **2007**, *9*, 3416.
(41) Clark, S. J.; Segall, M. D.; Pickard, C. J.; Hasnip, P. J.; Probert, M. J.; Refson, K.; Payne, M. C. *Z. Kristallogr.* **2005**, *220*, 567.
(42) Al-Karaghouli, A. R.; Cole, F. E.; Lehmann, M. S.; Miskell, C. F.; Verbist, J. J.; Koetzle, T. F. *J. Chem. Phys.* **1975**, *63*, 1360.
(43) Stewart, R. F.; Jensen, L. H. *Acta Crystallogr.* **1967**, *23*, 1102.
(44) Troullier, N.; Martins, J. L. *Phys. Rev. B* **1991**, *43*, 1993.
(45) Uldry, A. C.; et al. *J. Am. Chem. Soc.* **2008**, *130*, 945.

J couplings were calculated as described by Joyce et al. using a developer version of the CASTEP software package:[46] Trouiller−Martins norm-conserving pseudopotentials[44] are used together with the projector augmented wave (PAW)[47] technique in order to recover the all-electron accuracy. The exchange-correlation functional employed was the Perdew−Burke−Ernzerhof (PBE)[48] implementation of the generalized gradient approximation. The *J* coupling calculations were performed with a plane-wave cutoff of 1100 eV and a *k*-point sampling grid density of 0.09 (glycine·HCl) or 0.08 (uracil) Å^{-1}. The *J* couplings are computed by considering one nucleus as a perturbation, and it is therefore necessary to multiply the size of the original crystal unit cell until the values of the couplings are converged. A 2 × 2 × 1 supercell (192 atoms) and a 2 × 2 × 2 supercell (384 atoms) were found to be sufficient for the *J* couplings to be well converged within ±0.1 Hz for glycine·HCl and uracil, respectively. For uracil, the calculation time for the *J* couplings varied between 27 and 41 h on 24 nodes of the AMD Opteron cluster at St. Andrews University, depending on the perturbing nucleus.

3. Molecular Structures and 1D MAS NMR Spectra

The arrangement of glycine and uracil molecules in the geometrically optimized (CASTEP) crystal structures of glycine·HCl[42] and uracil[43] is illustrated in Figure 2. The intramolecular C−O distances in glycine·HCl, as well as the closest intra- and intermolecular N−O distances in glycine·HCl and uracil, are indicated. The N−O distances are listed in Table 1, which also specifies the corresponding dipolar coupling constants in hertz:

$$D_{jk} = -\frac{\mu_0 \gamma_j \gamma_k \hbar}{8\pi^2 r_{jk}^3} \quad (1)$$

where r_{jk} is the internuclear distance between spins *j* and *k*, and γ_j and γ_k are the respective gyromagnetic ratios of *j* and *k*.

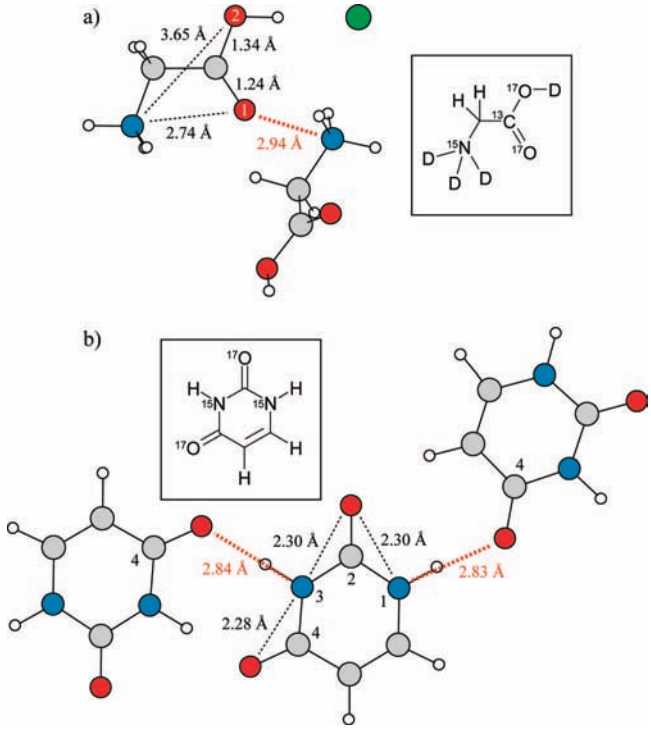

Figure 2. Representations of the geometrically optimized (CASTEP) crystal structures of (a) glycine·HCl[42] and (b) uracil.[43] Color coding: H, white; C, gray; N, blue; O, red; Cl, green. The closest intramolecular (in black) and intermolecular (in red) distances are indicated. The isotopically enriched sites in both molecules are labeled within the insets.

Table 1. Intra- and Intermolecular[a] N−O Proximities[b] in Glycine·HCl and Uracil

sample	*j*	*k*	r_{jk} /Å	$\lvert D_{jk}\rvert$ /Hz
glycine·HCl	N	O1	2.74	80
	N	**O1**	**2.94**	**65**
	N	O2	3.65	34
uracil	N1	O2	2.30	135
	N1	**O4**	**2.83**	**73**
	N3	O2	2.30	136
	N3	O4	2.28	139
	N3	**O4**	**2.84**	**72**

[a] Intermolecular distances are highlighted using boldface type. [b] Distances are from the geometrically optimized (CASTEP) crystal structures.

For the nitrogen atom in glycine·HCl, the closest intermolecular N−O proximity of 2.94 Å to O1 (C═O) is longer than the intramolecular N−O proximity of 2.74 Å. For O2 (C−OH), the closest proximity is the intramolecular N−O distance of 3.65 Å, with the nearest intermolecular proximity being at 4.15 Å. In uracil, there are three short intramolecular N−O distances (2.28−2.30 Å), with N3 being sandwiched between two C═O groups and hence having two close intramolecular N−O proximities as compared to the one for N1. Both N1 and N3 form intermolecular NH···O hydrogen bonds to O4 with N−O distances of 2.83 and 2.84 Å (Figure 2b). While O4 takes part in NH···O hydrogen bonds with both N1 *and* N3, O2 forms weak CH···O hydrogen bonds, which have been the subject of a recent combined experimental and first-principles computational study;[45] note the different atom numbering convention in ref 45 as compared to the present work.

It is evident that the N−O proximities in glycine·HCl and uracil do not correspond to well-isolated spin pairs. In this case, it is informative to consider the root-sum-squared dipolar coupling:[49]

$$D_{\mathrm{rss},j} = \sqrt{\sum_{k \neq j} D_{jk}^2} \quad (2)$$

which, in analogy to a second moment analysis, is a measure of the "effective coupling" at a particular site. Specifically, $D_{\mathrm{rss},j}$ is related to the second moment (for heteronuclear dipolar coupled nuclei) by[50]

$$M_2 = (4/15) I(I+1)(2\pi)^2 D_{\mathrm{rss},j}^2 \quad (3)$$

where *I* is the spin quantum number of the nuclear spins coupled to nucleus *j*. $D_{\mathrm{rss},j}$ values for the dipolar couplings of the ^{15}N nuclei in glycine·HCl and uracil to the surrounding oxygen nuclei (considering N−O distances up to 6.0 Å) are listed in Table 2. However, it is to be noted that the oxygen sites are only partially ^{17}O labeled. Assuming the isotopic labels are randomly distributed, Zorin et al. have shown (see eq 6 of ref 51) that

$$D_{\mathrm{rss},j}(\rho) = \sqrt{\rho} D_{\mathrm{rss},j} \quad (4)$$

where ρ denotes the proportion of labeled nuclei.

(46) Joyce, S. A.; Yates, J. R.; Pickard, C. J.; Mauri, F. *J. Chem. Phys.* **2007**, *127*, 204107.
(47) Blochl, P. E. *Phys. Rev. B* **1994**, *50*, 17953.
(48) Perdew, J. P.; Burke, K.; Ernzerhof, M. *Phys. Rev. Lett.* **1996**, *77*, 3865.
(49) Zorin, V. E.; Brown, S. P.; Hodgkinson, P. *Mol. Phys.* **2006**, *104*, 293.
(50) van Wullen, L.; Muller, U.; Jansen, M. *Chem. Mater.* **2000**, *12*, 2347.

Table 2. N−O Root-Sum-Squared Dipolar Couplings Determined from the Geometrically Optimized (CASTEP) Crystal Structures of Glycine·HCl and Uracil

sample	*j*	*k*	$D_{rss,j}$/Hz[a]
glycine·HCl	N	O1	108
	N	O2	58
	N	O1, O2	123
	O1	N	108
	O2	N	58
uracil	N1	O2	149
	N1	O4	87
	N1	O2, O4	173
	N3	O2	142
	N3	O4	166
	N3	O2, O4	219

[a] As defined in eq 2, considering all distances up to 6.0 Å.

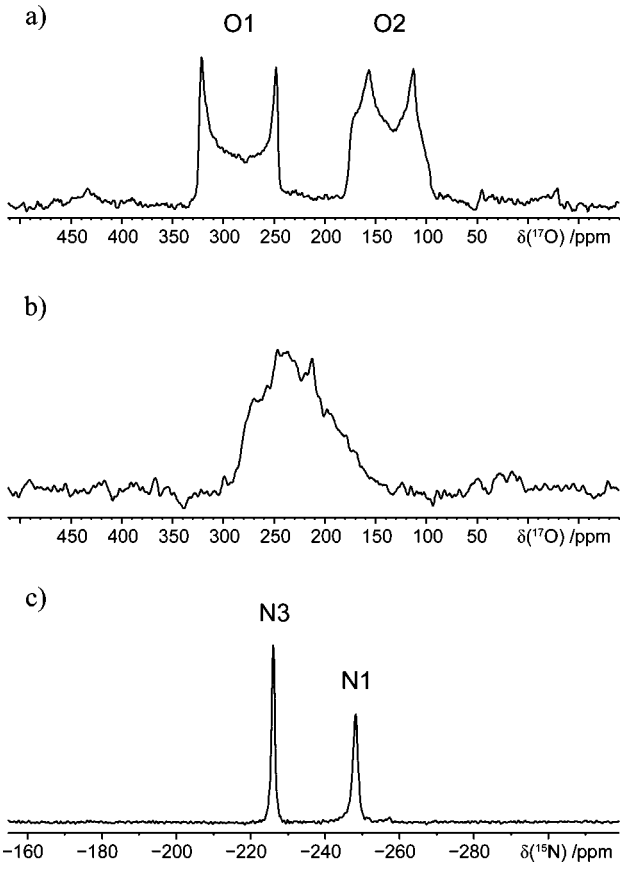

Figure 3. ^{17}O MAS NMR spectra of (a) [^{2}H(NH$_3$),1-^{13}C,^{15}N,^{17}O$_2$]glycine·^{2}HCl (ν_r = 22.5 kHz) and (b) [^{15}N$_2$,^{17}O$_2$]uracil (ν_r = 20.0 kHz). (c) ^{15}N CP/MAS spectrum of [^{15}N$_2$,^{17}O$_2$]uracil at ν_r = 10.0 kHz. All spectra were recorded at 14.1 T (ν_0(^{1}H) = 600 MHz). A total of (a) 256, (b) 2400, and (c) 4 transients were coadded. RAPT[28] (n = 3, ν_{off} = 450 kHz) was used for signal enhancement of ^{17}O spectra.

^{13}C and ^{15}N CP/MAS spectra (not shown) of the labeled glycine·^{2}HCl sample both show a single resonance at 172.6 and −343.5 ppm, respectively, while two well-resolved quadrupolar patterns corresponding to the two distinct COO^{2}H group ^{17}O sites are observed in a ^{17}O MAS spectrum at 14.1 T (Figure 3a). The ^{17}O resonances centered at approximately 280 and 130 ppm are assigned to the C═O (O1) and C−O^{2}H (O2) sites, respectively.[23,52] In contrast, for the labeled uracil sample, the signals from the O2 and O4 sites cannot be resolved in a ^{17}O MAS NMR spectrum at 14.1 T, which shows a single broadened pattern centered at 230 ppm (Figure 3b). Overlap of the signals is caused by the similarity in chemical shifts and quadrupolar parameters for the two oxygen nuclei, which have previously been studied by ^{17}O MQMAS.[25] The isotropic chemical shifts and quadrupolar parameters for the ^{17}O sites in glycine·^{2}HCl and uracil are listed in Table 3. The ^{15}N CP/MAS spectrum of uracil shows two signals at −244.2 and −222.2 ppm which are assigned to the N1 and N3 sites (Figure 3c).[45]

Table 3. ^{17}O Isotropic Chemical Shift and Quadrupolar Parameters for Glycine·^{2}HCl and Uracil

sample	site	δ_{iso}/ppm	C_Q/MHz[c]	η_Q
glycine·^{2}HCl[a]	O1	334	8.34	0.00
	O2	175	7.48	0.24
uracil[b]	O2	240	7.62	0.50
	O4	275	7.85	0.55

[a] Parameters taken from ref 23. [b] Parameters taken from ref 25. [c] $C_Q = e^2qQ/h$, where eq is the electric field gradient and Q is the nuclear quadrupole moment.

4. Two-Dimensional Through-Space Correlation Experiments

Recently, heteronuclear multiple-quantum correlation (HMQC)[53] solid-state NMR experiments have been presented that correlate the chemical shift evolution of coupled spin I = 1/2 and quadrupolar nuclei, with applications to ^{1}H/^{14}N,[29,54] ^{13}C/^{14}N,[55,56] ^{31}P/^{23}Na,[30] ^{1}H/^{27}Al,[30] and ^{31}P/^{27}Al[30] having been reported. One demonstrated method for establishing such heteronuclear correlations is the use of rotary-resonance recoupling (R^3)[57] to recouple the heteronuclear dipolar coupling that would otherwise be averaged to zero by MAS. In the R^3 method, radio frequency (rf) irradiation of duration $N\tau_r$ reintroduces homonuclear dipolar coupling, heteronuclear dipolar coupling, and/or chemical-shift anisotropy depending on the ratio of the applied rf frequency and the rotation frequency, $\nu_1 = n\nu_r$ (n = 1/2, 1, 2).[29] The n = 1 R^3 condition is most efficient and recouples both the homo- and heteronuclear dipolar interactions; hence, it is employed in the present cases since the effect of homonuclear ^{15}N couplings is generally expected to be weak. The application of R^3 has been thoroughly discussed elsewhere,[29,30,57] and its comparison with other heteronuclear dipolar recoupling methods has recently been reported.[58] The simplicity of applying R^3 stems from the limited number of variables required for its optimization. Having chosen which $\nu_1 = n\nu_r$ R^3 condition to employ, only the recoupling pulse length (τ/2) remains to be determined. In both instances presented herein, the maximum ^{17}O R^3-HMQC intensity (∼5−7% compared to a spin−echo experiment) was observed when τ/2 was ap-

(51) Zorin, V. E.; Brown, S. P.; Hodgkinson, P. *J. Chem. Phys.* **2006**, *125*, 144508.
(52) Pike, K. J.; Lemaitre, V.; Kukol, A.; Anupold, T.; Samoson, A.; Howes, A. P.; Watts, A.; Smith, M. E.; Dupree, R. *J. Phys. Chem. B* **2004**, *108*, 9256.
(53) Muller, L. *J. Am. Chem. Soc.* **1979**, *101*, 4481.
(54) Cavadini, S.; Abraham, A.; Bodenhausen, G. *Chem. Phys. Lett.* **2007**, *445*, 1.
(55) Gan, Z. H. *J. Magn. Reson.* **2007**, *184*, 39.
(56) Cavadini, S.; Antonijevic, S.; Lupulescu, A.; Bodenhausen, G. *ChemPhysChem* **2007**, *8*, 1363.
(57) Oas, T. G.; Griffin, R. G.; Levitt, M. H. *J. Chem. Phys.* **1988**, *89*, 692.
(58) Hu, B.; Trebosc, J.; Amoureux, J. P. *J. Magn. Reson.* **2008**, *192*, 112.

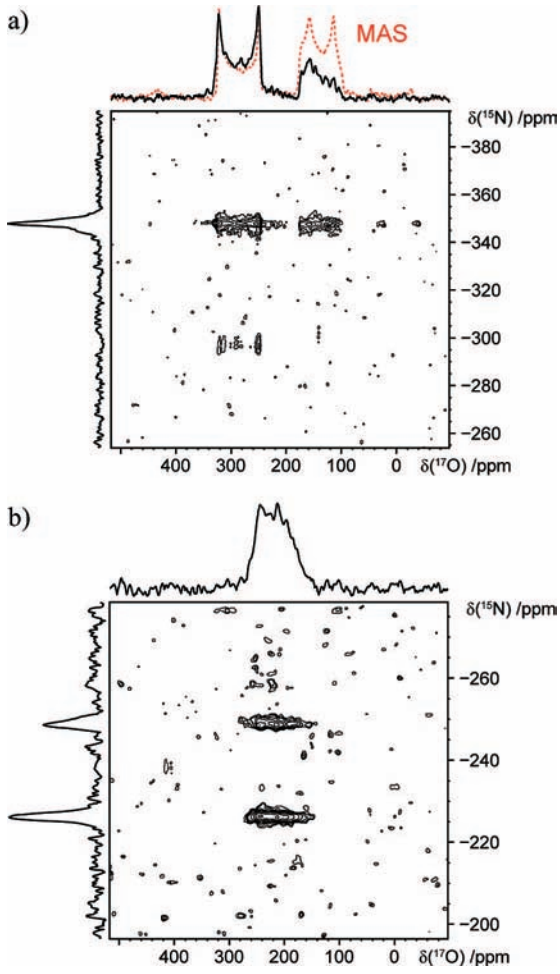

Figure 4. 2D $^{17}O/^{15}N$ R^3-HMQC NMR spectra of (a) [$^2H(NH_3)$,1-^{13}C,^{15}N,$^{17}O_2$]glycine·^{2}HCl and (b) [$^{15}N_2$,$^{17}O_2$]uracil with skyline projections along F_1 and F_2. The base contours are set at 12% and 20% of the maximum intensity for spectra a and b, respectively. The ^{17}O MAS spectrum (dotted red line) of [$^2H(NH_3)$, 1-^{13}C,^{15}N,$^{17}O_2$]glycine·^{2}HCl is superimposed over the F_2 projection in spectrum a for comparison.

proximately equal to the inverse of the effective dipolar coupling (see section 3).

A 2D $^{17}O/^{15}N$ R^3-HMQC NMR spectrum for glycine·^{2}HCl acquired using the sequence in Figure 1a is shown in Figure 4a. A clear correlation between the ^{15}N site and both ^{17}O resonances can be observed, attesting to the proximities between the nitrogen and both oxygen nuclei. The projection along the ^{17}O dimension provides an accurate representation of the O1 pattern when compared to the ^{17}O MAS spectrum, whereas the O2 signal shows less resemblance—this may be due to the poorer signal intensity. The relative intensities of the two correlation peaks show a qualitative correspondence with the relative distance between the ^{15}N and the O1 (2.7 Å) and O2 (3.7 Å) sites (Figure 2a) as well as the effective dipolar couplings considering all N−O1 and N−O2 distances under 6 Å, $D_{rss,j}$(N−O1) = 108 and $D_{rss,j}$(N−O2) = 58 Hz (see Table 2). The $^{17}O/^{15}N$ R^3-HMQC spectrum for uracil also shows two distinct correlation peaks (Figure 4b). However, in this instance the two oxygen sites cannot be distinguished (see the ^{17}O MAS spectrum in Figure 3b); hence, it can only be stated that there are spatial proximities between each N site and at least one O site. In order to separate the different quadrupolar patterns, a high-resolution method such as MQMAS[59] or STMAS[60] would have to be included into the HMQC experiment, as has been suggested in the literature.[61] The spectra presented here demonstrate the feasibility of observing $^{15}N-^{17}O$ R^3-HMQC heteronuclear correlations for N−O spatial proximities out to 3.7 Å; i.e., heteronuclear correlations between ^{15}N and ^{17}O can be obtained with dipolar couplings as small as ∼35 Hz.

5. Quantitative Measurement of Root-Sum-Squared Through-Space Dipolar Couplings

The above section has shown that heteronuclear spatial proximities can be observed in a semiquantitative fashion via 2D correlation experiments. This section presents $^{17}O-^{15}N$ rotational-echo double-resonance (REDOR)[62,63] and $^{15}N-^{17}O$ rotational-echo adiabatic-passage double-resonance (REAPDOR)[14,33,35] experimental buildup data for glycine·^{2}HCl and uracil, from which root-sum-squared dipolar couplings can be quantitatively determined.

5.1. $^{17}O-^{15}N$ REDOR Experiments. The REDOR fraction is given as $\Delta S/S = (S - S_r)/S$, where the r subscript in S_r refers to the reduced signal intensity in the dephased (under the heteronuclear dipolar coupling) spectrum, while S refers to the reference spectrum. For a pair of dipolar-coupled spin $I = 1/2$ nuclei, it is well established that the REDOR fraction depends only on the evolution time ($\tau = N\tau_r$) and the dipolar coupling constant D_{jk}, with this simple relation explaining the very widespread application of the REDOR experiment.[63] However, the ^{15}N and ^{17}O nuclei in glycine·HCl and uracil do not exist as well-isolated spin pairs (see section 3). For IS_n systems, the analysis is considerably complicated by the dependence of the REDOR response on the relative orientation of the internuclear vectors corresponding to the different IS heteronuclear dipolar couplings.[64−68] However, starting with the expression of Mueller for the initial REDOR buildup (for $\Delta S/S < 0.2$, where $\cos(x)$ can be expressed as $1 - x^2/2$),[69]

$$\Delta S/S = \frac{16N^2\tau_r^2}{15}\sum_{k\neq j} D_{jk}^2 = \frac{16N^2\tau_r^2}{15} D_{rss,j}^2 \qquad (5)$$

Eckert and co-workers have shown that the initial buildup of a REDOR experiment ($\Delta S/S < 0.2$) can be fit to the following parabolic function (using the definition of the second moment in eq 3):[70−72]

$$\Delta S/S = \frac{N^2\tau_r^2}{\pi^2 I(I+1)} M_2 \qquad (6)$$

(59) Frydman, L.; Harwood, J. S. *J. Am. Chem. Soc.* **1995**, *117*, 5367.
(60) Gan, Z. H. *J. Am. Chem. Soc.* **2000**, *122*, 3242.
(61) Amoureux, J. P.; Trebosc, J.; Wiench, J.; Pruski, M. *J. Magn. Reson.* **2007**, *184*, 1.
(62) Gullion, T.; Schaefer, J. *J. Magn. Reson.* **1989**, *81*, 196.
(63) Gullion, T. *Concepts Magn. Reson.* **1998**, *10*, 277.
(64) Naito, A.; Nishimura, K.; Tuzi, S.; Saito, H. *Chem. Phys. Lett.* **1994**, *229*, 506.
(65) Goetz, J. M.; Schaefer, J. *J. Magn. Reson.* **1997**, *127*, 147.
(66) Brouwer, E. B.; Gougeon, R. D. M.; Hirschinger, J.; Udachin, K. A.; Harris, R. K.; Ripmeester, J. A. *Phys. Chem. Chem. Phys.* **1999**, *1*, 4043.
(67) Nishimura, K.; Naito, A.; Tuzi, S.; Saito, H. *J. Phys. Chem. B* **1999**, *103*, 8398.
(68) Fyfe, C. A.; Lewis, A. R. *J. Phys. Chem. B* **2000**, *104*, 48.
(69) Mueller, K. T. *J. Magn. Reson. Ser. A* **1995**, *113*, 81.
(70) Bertmer, M.; Eckert, H. *Solid State Nucl. Magn. Reson.* **1999**, *15*, 139.
(71) Chan, J. C. C.; Bertmer, M.; Eckert, H. *J. Am. Chem. Soc.* **1999**, *121*, 5238.
(72) Bertmer, M.; Zuchner, L.; Chan, J. C. C.; Eckert, H. *J. Phys. Chem. B* **2000**, *104*, 6541.

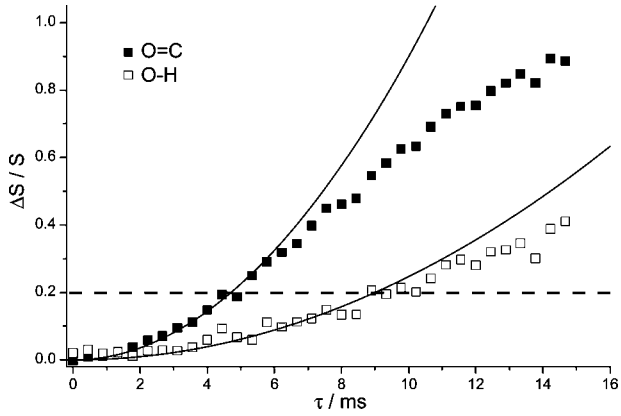

Figure 5. Experimental $^{17}O/^{15}N$ REDOR curves, $\Delta S/S = (S - S_r)/S$, as a function of the dephasing time for the O1 (C═O) (filled squares) and O2 (O^2H) (open squares) resonances of [$^2H(NH_3)$,1-^{13}C,^{15}N,$^{17}O_2$]glycine·^{2}HCl. The best fits to eq 5 for $\Delta S/S < 0.2$ (horizontal dashed line) are shown as solid lines.

where I is the spin-quantum number of the nonobserve nucleus. The validity of eq 6 has been demonstrated by simulations of IS_n systems with different geometries[70,71] and $^{23}Na/^{31}P$ and $^{27}Al/^{31}P$ REDOR experiments on sodium and aluminum phosphates for which the fitted second moments are within 10% of those calculated using the known crystal structures.[32] This approach has subsequently been employed in the quantitative analysis of $^{29}Si/^{1}H$, $^{23}Na/^{31}P$, and $^{6}Li/^{31}P$ REDOR data for zeolites,[73] glasses,[74,75] and lithium ion site dynamics.[76] Moreover, Strojek et al. have shown that the approach can be extended to REDOR experiments for a $I = 3/2$ nonobserve nucleus, whereby it is necessary to include a coefficient (determined from simulations that require only an estimate of the C_Q and η_Q of the quadrupolar nucleus) to take into account the incomplete inversion of the satellite transitions.[77]

Experimental $^{17}O/^{15}N$ REDOR buildup data obtained using the pulse sequence in Figure 1b for the carbonyl ^{17}O (O1) and hydroxyl ^{17}O (O2) resonances of glycine·^{2}HCl are shown in Figure 5. The slower dephasing for the hydroxyl resonance—consistent with the $D_{rss,j}$ values in Table 2—is evident when comparing the buildup curves for O1 and O2 in Figure 5. Best fits ($\Delta S/S < 0.2$) to eq 5—shown as solid lines—yield fitted values for $D_{rss,j}$ of 89 ± 9 and 46 ± 6 Hz for the carbonyl and hydroxyl resonances, respectively, corresponding to 82% and 79% of the values determined from the crystal structure (see Table 2).

5.2. $^{15}N-^{17}O$ REAPDOR Experiments. The REAPDOR experiment (Figure 1c) is a modification of the REDOR experiment that allows the quantitative determination of the heteronuclear dipolar coupling between spin $I = 1/2$ nuclei (observe) and quadrupolar nuclei. Considering half-integer quadrupolar nuclei, REAPDOR experiments have been performed for various combinations of nuclei: $^{1}H/^{23}Na$,[78] $^{1}H/^{27}Al$,[78−81] $^{13}C/^{11}B$,[82] $^{13}C/^{17}O$,[14−16,34] $^{13}C/^{27}Al$,[79] $^{13}C/^{67}Zn$,[34] $^{15}N/^{23}Na$,[78] $^{15}N/^{27}Al$,[78] $^{29}Si/^{11}B$,[50,82,83] $^{29}Si/^{23}Na$,[84] $^{29}Si/^{27}Al$,[85] $^{31}P/^{27}Al$,[86−88] $^{31}P/^{45}Sc$,[89] $^{31}P/^{51}V$,[90] and $^{31}P/^{59}Co$.[91] Their applications include a tripeptide,[16] a metal−nucleotide complex,[91] zeolites,[78−81,84,85] ceramics,[50,82] glasses,[83,87−89] and vanadium-substituted polyoxoanionic solids.[90]

In the REDOR experiment, dephasing due to the heteronuclear dipolar coupling relies on π inversion pulses applied every half a rotor period, so as to recouple the dipolar coupling that would otherwise be averaged to zero by MAS over one complete rotor period.[62,63] For quadrupolar nuclei, it is often the case that the quadrupolar broadening extends over megahertz for powdered samples, such that at usual rf nutation frequencies it is not possible to achieve a uniform inversion of the broad distribution of orientation-dependent resonances. In the REAPDOR experiment, an enhanced dephasing as compared to a REDOR experiment[15,50] is achieved by replacing the π pulse on the quadrupolar nucleus by a so-called adiabatic-passage pulse. Specifically, such a pulse achieves a transfer of populations among the m states of the quadrupolar nuclei by means of the avoided level crossings that link different eigenstates of the quadrupolar Hamiltonian. These avoided level crossings can occur when the quadrupolar splitting changes sign, i.e., goes through zero, as a consequence of MAS−the $\cos(\omega_r t)$ and $\cos(2\omega_r t)$ dependence means that there are two or four zero-crossings per rotor period, depending on the orientation of the quadrupolar tensor.[35,92] When a spin changes its eigenstate at such a zero-crossing, the passage is said to be adiabatic, with the likelihood of an adiabatic passage depending on the adiabaticity parameter:[93−95]

$$\alpha = \nu_1^2/\nu_Q\nu_r \tag{7}$$

where

$$\nu_Q = 3C_Q/[2I(2I-1)]$$
$$= 3C_Q/20 \qquad \text{for } I = 5/2 \tag{8}$$

For a spin $I = 5/2$ nucleus, experiment and simulation has shown that the adiabaticity parameter must exceed 0.55.[15,34] The adiabatic pulse is set to be of duration $\tau_r/3$, since this corresponds to the maximizing of the number of crystallites in a powder making a single zero-crossing (NB: an even number of crossings

(73) Magusin, P. C. M. M.; Zorin, V. E.; Aerts, A.; Houssin, C. J. Y.; Yakovlev, A. L.; Kirschhock, C. E. A.; Martens, J. A.; van Santen, R. A. *J. Phys. Chem. B* **2005**, *109*, 22767.
(74) Santagneli, S. H.; de Araujo, C. C.; Strojek, W.; Eckert, H.; Poirier, G.; Ribeiro, S. J. L.; Messaddeq, Y. *J. Phys. Chem. B* **2007**, *111*, 10109.
(75) Strojek, W.; Fehse, C. M.; Eckert, H.; Ewald, B.; Kniep, R. *Solid State Nucl. Magn. Reson.* **2007**, *32*, 89.
(76) Cahill, L. S.; Kirby, C. W.; Goward, G. R. *J. Phys. Chem. C* **2008**, *112*, 2215.
(77) Strojek, W.; Kalwei, M.; Eckert, H. *J. Phys. Chem. B* **2004**, *108*, 7061.
(78) Holland, G. P.; Alam, T. M. *Phys. Chem. Chem. Phys.* **2005**, *7*, 1739.
(79) van Wullen, L.; Koller, H.; Kalwei, M. *Phys. Chem. Chem. Phys.* **2002**, *4*, 1665.
(80) Ganapathy, S.; Kumar, R.; Delevoye, L.; Amoureux, J. P. *Chem. Commun.* **2003**, 2076.
(81) Kalwei, M.; Koller, H. *Solid State Nucl. Magn. Reson.* **2002**, *21*, 145.
(82) van Wullen, L.; Jansen, M. *J. Mater. Chem.* **2001**, *11*, 223.
(83) van Wullen, L.; Schwering, G. *Solid State Nucl. Magn. Reson.* **2002**, *21*, 134.
(84) Ganapathy, S.; Vega, S. *J. Am. Chem. Soc.* **1998**, *120*, 1078.
(85) Ganapathy, S.; Kumar, R.; Montouillout, V.; Fernandez, C.; Amoureux, J. P. *Chem. Phys. Lett.* **2004**, *390*, 79.
(86) van Wullen, L.; Tricot, G.; Wegner, S. *Solid State Nucl. Magn. Reson.* **2007**, *32*, 44.
(87) Zhang, L.; Eckert, H. *J. Phys. Chem. B* **2006**, *110*, 8946.
(88) Wegner, S.; van Wullen, L.; Tricot, G. *J. Non-Cryst. Solids* **2008**, *354*, 1703.
(89) Mohr, D.; de Camargo, A. S. S.; de Araujo, C. C.; Eckert, H. *J. Mater. Chem.* **2007**, *17*, 3733.
(90) Huang, W. L.; Vega, A. J.; Gullion, T.; Polenova, T. *J. Am. Chem. Soc.* **2007**, *129*, 13027.
(91) Grant, C. V.; Frydman, V.; Harwood, J. S.; Frydman, L. *J. Am. Chem. Soc.* **2002**, *124*, 4458.
(92) Ba, Y.; Kao, H. M.; Grey, G. P.; Chopin, L.; Gullion, T. *J. Magn. Reson.* **1998**, *133*, 104.

during a rotor period would leave the spin in the same eigenstate).[92]

As compared to the REDOR experiment,[63] the REAPDOR fraction, $\Delta S/S = (S - S_r)/S$, is not a simple function of the dipolar coupling constant because the quadrupolar spin flips are more complex than a simple inversion of their z-component, with the adiabatic pulse inducing partial transitions among the magnetic spin states m of the quadrupolar nuclei, rather than effecting a uniform 180° inversion.[96] However, an advantage of the REAPDOR experiment is that there is only a slight dependence of the REAPDOR fraction on the orientation of the quadrupolar tensor with respect to the internuclear vector, with the latter being difficult to determine experimentally.[81] Indeed, Goldbourt et al. have shown that for a spin $I = 1/2$ nucleus coupled to a spin $I = 5/2$ nucleus, there exists a universal REAPDOR curve (valid when $\alpha > 0.55$ for an adiabatic pulse of duration $\tau_r/3$):[34]

$$\Delta S/S = 0.63(1 - \exp[-(3.0D_{jk}\tau)^2]) + 0.2(1 - \exp[-(0.7D_{jk}\tau)^2]) \quad (9)$$

Specifically, simulated curves for C_Q between 1 and 13 MHz, η_Q between 0 and 1, ν_1 between 40 and 150 kHz, and ν_r between 3 and 20 kHz (for a range of orientations of the quadrupolar tensor with respect to the internuclear vector) were shown to not deviate (for $D_{jk}\tau < 0.5$) more than 15% from the universal curve.[34]

Experimental $^{15}N/^{17}O$ CP/REAPDOR buildup data for glycine·^{2}HCl and uracil are shown in Figure 6. Experiments were performed at different MAS frequencies, with the adiabaticity parameter in all cases exceeding 0.55: for glycine·^{2}HCl, $\nu_r = 3.5$ ($\alpha \approx 1.3$), 5.0 ($\alpha \approx 0.9$), and 8.0 ($\alpha \approx 0.6$) kHz; for uracil, $\nu_r = 6.5$ ($\alpha \approx 0.75$) and 7.0 ($\alpha \approx 0.70$) kHz; see Table 3 for C_Q values, $\nu_1(^{17}O) = 75$ kHz. Best fits to eq 9 are shown as solid lines, with dashed lines corresponding to a ±15% variation of the best-fit dipolar coupling (Table 4). Within the stated range of validity of eq 9, i.e., $D_{jk}\tau < 0.5$, the experimental points are observed to nearly all be within the ±15% bounds of the universal REAPDOR curve (eq 9). In this context, whereas in ref 34 experimental REAPDOR data are presented for well-isolated $^{13}C-^{67}Zn$ and $^{13}C-^{17}O$ spin pairs, van Wüllen et al. have shown by simulation that $^{29}Si/^{11}B$ REAPDOR curves for IS_2 systems are insensitive to geometry (for $\Delta S/S < 0.5$).[50] Moreover, $^{13}C-^{17}O$ REAPDOR buildup data for the tripeptide L-alanyl-alanyl-alanine in an antiparallel β-sheet arrangement have been shown to fit well to eq 9 using a single effective dipolar coupling.[16]

The fitted effective dipolar couplings in Table 4 are all observed to be significantly smaller than those determined from the geometrically optimized (CASTEP) crystal structures (see Table 2); this is a consequence of the partial ^{17}O labeling. Rearranging eq 4, it follows that

$$\rho = \frac{D_{rss,j}(\rho)^2}{D_{rss,j}(\text{crystal})^2} \quad (10)$$

The proportions of ^{17}O-labeled nuclei ρ in the glycine·^{2}HCl and uracil samples, as determined using eq 10 from the fitted effective dipolar couplings for the $^{15}N/^{17}O$ CP/REAPDOR buildup data in Figure 6, are listed in Table 4. While both samples were prepared using [70%-^{17}O]H_2O, the uracil sample is found to have a considerably lower degree of ^{17}O labeling. In this respect, it is to be noted that the uracil sample was prepared following the method described by Wu and co-workers, who estimated the degree of labeling in their sample as 14% at O2 and 24% at O4, starting with [40%-^{17}O]H_2O.[25] This observation of non-uniform ^{17}O labeling is consistent with the lower ρ extracted for the N1 (0.11 ± 0.04) as compared to the N3 (0.26 ± 0.08) uracil REAPDOR curves: From inspection of the molecular structure, N1 has one close intramolecular proximity to O2, while N2 has close intramolecular proximities to O2 and O4.

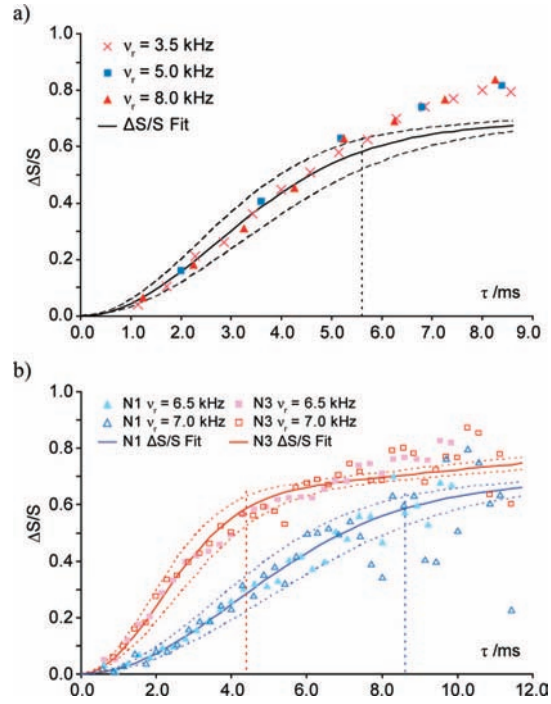

Figure 6. Experimental $^{15}N/^{17}O$ CP/REAPDOR curves, $\Delta S/S = (S - S_r)/S$, as a function of the dephasing time for (a) [$^2H(NH_3)$,1-^{13}C,^{15}N,$^{17}O_2$]glycine·^{2}HCl and (b) [$^{15}N_2$,$^{17}O_2$]uracil at various MAS frequencies. The best fits (assuming a single effective dipolar coupling, see Table 4) to eq 9 are shown as solid lines, with dashed lines corresponding to a ±15% variation of the best-fit dipolar coupling. Vertical dotted lines indicate the regions corresponding to $D_{jk}\tau < 0.5$ (see Table 4). The error bars for the signal intensity in experiments acquired with (S_r) and without (S) the dephasing pulse(s) were determined to be ±0.006 (glycine·^{2}HCl) and ±0.02 (uracil).

Table 4. $^{15}N-^{17}O$ Dipolar Coupling Parameters for Glycine·^{2}HCl and Uracil

site	D_{jk} ± 15%/Hz[a]	$D_{rss,j}$/Hz[b]	ρ[c]	τ ($D_{jk}\tau = 0.5$)/ms
glycine·^{2}HCl N	88 ± 13	123	0.37−0.68	5.6
uracil N1	58 ± 9	173	0.08−0.15	8.6
uracil N3	114 ± 17	219	0.20−0.36	4.4

[a] Determined from fits of the $^{15}N-^{17}O$ REAPDOR data in Figure 6 to eq 9. [b] As defined in eq 2, considering all N−O distances up to 6.0 Å in the geometrically optimized (CASTEP) crystal structures. [c] Determined using eq 10.

6. Quantitative Measurement of Through-Bond *J* Couplings

J couplings are not normally resolved in ordinary one-dimensional solid-state NMR spectra, since the observed line

(93) Vega, A. J. *J. Magn. Reson.* **1992**, *96*, 50.
(94) Grey, C. P.; Veeman, W. S.; Vega, A. J. *J. Chem. Phys.* **1993**, *98*, 7711.
(95) Grey, C. P.; Vega, A. J. *J. Am. Chem. Soc.* **1995**, *117*, 8232.
(96) Hughes, E.; Gullion, T.; Goldbourt, A.; Vega, S.; Vega, A. J. *J. Magn. Reson.* **2002**, *156*, 230.

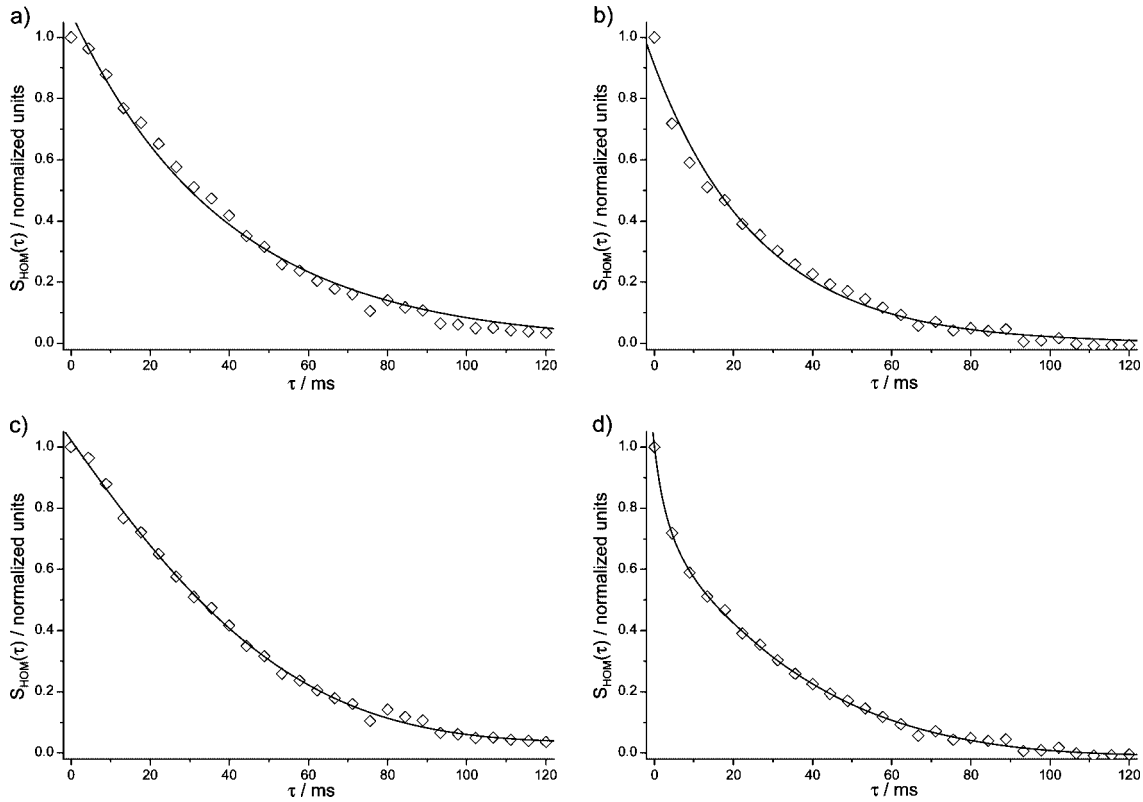

Figure 7. ^{17}O homonuclear spin−echo ($\tau/2-\pi-\tau/2$) intensities for the (a,c) carbonyl (O1) and (b,d) hydroxyl (O2) ^{17}O resonances in [^{2}H(NH$_3$),1-^{13}C,^{15}N,^{17}O$_2$]glycine·^{2}HCl as a function of the evolution time together with best fits (solid lines, see Table 5) to (a,b) eq 11 and (c,d) eq 12. Experiments were carried out at 14.1 T ($\nu_0(^1\text{H}) = 600$ MHz) and a MAS frequency of 22.5 kHz. The error bars for the experimental intensities were determined to be ±0.02 and are omitted for clarity.

Table 5. Parameters Extracted from the Fits of the ^{17}O Glycine·^{2}HCl Homonuclear Spin−Echo ($\tau/2-\pi-\tau/2$) Intensities in Figure 7

data set	A	p^a	T_{2a}'/ms	J_{OO}/Hz	T_{2b}'/ms	$[\varepsilon^2]^b$
S_{HOM} O1 (C═O)^c	1.08 ± 0.01		39.2 ± 0.7			0.0037
S_{HOM} O2 (O^{2}H)^c	0.91 ± 0.01		26.8 ± 0.6			0.0076
S_{HOM} O1 (C═O)^{d,e}	1.02 ± 0.01	0.34 ± 0.03	56.1 ± 4.2	8.8 ± 0.9	56.1^f ± 4.2	0.0009
S_{HOM} O2 (O^{2}H)^{d,e}	1.00 ± 0.02	0.73 ± 0.04	40.2 ± 3.9	4.5 ± 0.4	3.1 ± 1.1	0.0007

^{a} The proportion of ^{17}O nuclei with an intramolecular $^2J_{OO}$ coupling, i.e., corresponding to the proportion of ^{17}O-labeled nuclei. ^{b} $\varepsilon^2 = \sum[I_{fit}(n) - I_{exp}(n)]^2/\sum I_{exp}(n)^2$. ^{c} Fit to eq 11. ^{d} Fit to eq 12. ^{e} One or more correlation coefficients are greater than 0.7 (see Supporting Information). ^{f} T_{2a}' was set equal to T_{2b}' (otherwise correlation coefficients of greater than 0.99 were obtained).

width is usually larger than the magnitude of the coupling. However, a simple $\tau/2-\pi-\tau/2$ spin−echo MAS experiment refocuses evolution due to all terms that appear as offsets, e.g., magnetic field inhomogeneity or disorder, hence enabling the observation of J coupling modulation. The use of efficient heteronuclear decoupling gives transverse dephasing times, T_2', which are usually much longer than the decay constants of the non-refocused NMR signal, T_2*,[97,98] that characterize the free-induction decay. Hence, it is possible to obtain refocused line widths ($\Delta' = 1/\pi T_2'$) that are sufficiently narrow that splittings due to J couplings can be observed. J modulation in MAS spin−echo experiments has been the subject of theoretical analysis.[99−101] In particular, Duma et al. have provided a full theoretical treatment of spin−echo J modulation for a homonuclear pair of spin $I = 1/2$ nuclei, supported by numerical simulations and experimental results on model systems.[101] It was found that fitting the spin−echo modulation yields an accurate measurement of the J coupling constant, provided that, as is usually the case, rotational resonance conditions[102] are avoided. This is found to be true even in the presence of large anisotropic interactions such as the chemical shift anisotropy and homonuclear dipolar coupling, which surprisingly act to stabilize the spin−echo modulation rather than to perturb it. Heteronuclear J couplings can also be measured using a heteronuclear spin−echo experiment, with the determination of the J couplings between a spin $I = 1/2$ and a half-integer quadrupolar nucleus having been recently reported for the ^{31}P−^{27}Al[37,38] and ^{31}P−^{71}Ga[39] spin pairs.

(97) Cowans, B. A.; Grutzner, J. B. *J. Magn. Reson. Ser. A* **1993**, *105*, 10.
(98) Lesage, A.; Bardet, M.; Emsley, L. *J. Am. Chem. Soc.* **1999**, *121*, 10987.
(99) Kubo, A.; McDowell, C. A. *J. Chem. Phys.* **1990**, *92*, 7156.
(100) Challoner, R.; Nakai, T.; McDowell, C. A. *J. Chem. Phys.* **1991**, *94*, 7038.
(101) Duma, L.; Lai, W. C.; Carravetta, M.; Emsley, L.; Brown, S. P.; Levitt, M. H. *ChemPhysChem* **2004**, *5*, 815.
(102) Raleigh, D. P.; Levitt, M. H.; Griffin, R. G. *Chem. Phys. Lett.* **1988**, *146*, 71.
(103) Detken, A.; Hardy, E. H.; Ernst, M.; Meier, B. H. *Chem. Phys. Lett.* **2002**, *356*, 298.
(104) Griffin, J. M.; Tripon, C.; Samoson, A.; Filip, C.; Brown, S. P. *Magn. Reson. Chem.* **2007**, *45*, S198.

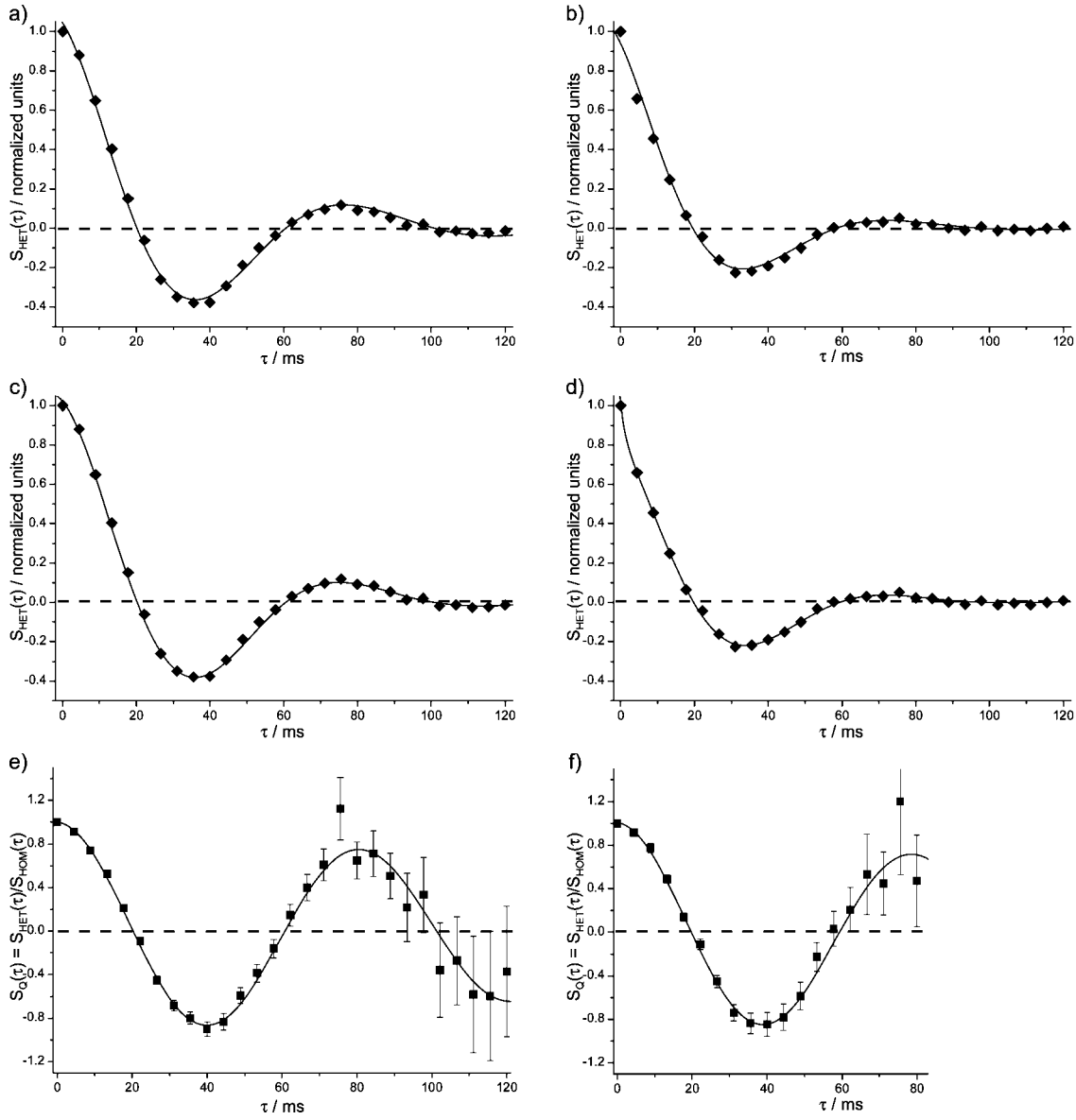

Figure 8. (a−d) $^{17}O/^{13}C$ heteronuclear spin−echo ($\tau/2-\pi-\tau/2$) intensities for the (a,c) carbonyl (O1) and (b,d) hydroxyl (O2) ^{17}O resonances in [$^2H(NH_3)$,1-^{13}C,^{15}N,$^{17}O_2$]glycine·^{2}HCl as a function of the evolution time together with best fits to (a,b) eq 13 and (c,d) eq 14 (solid lines, see Table 6). Experiments were carried out at 14.1 T ($\nu_0(^1H)$ = 600 MHz) and a MAS frequency of 22.5 kHz. The error bars for the experimental intensities were determined to be ±0.02 and are omitted for clarity. (e,f) The quotient $S_Q(\tau) = S_{HET}(\tau)/S_{HOM}(\tau)$ for the (e) carbonyl (O1) and (f) hydroxyl (O2) ^{17}O resonances in [$^2H(NH_3)$,1-^{13}C,^{15}N,$^{17}O_2$]glycine·^{2}HCl together with best fits to eq 15 (solid lines, see Table 6). $S_{HET}(\tau)$ and $S_{HOM}(\tau)$ refer to the $^{17}O/^{13}C$ heteronuclear and ^{17}O homonuclear spin−echo data presented in panels a and b of this figure and Figure 7, respectively. $S_Q(\tau)$ has been normalized such that $S_Q(\tau = 0) = 1.00$: experimentally the ratio of the integrated intensities $S_{HET}(\tau = 0)/S_{HOM}(\tau = 0)$ equaled 1.07 and 1.08 for the (e) carbonyl (O1) and (f) hydroxyl (O2) ^{17}O resonances, respectively.

Table 6. Parameters Extracted from the Fits of the $^{17}O-^{13}C$ Glycine·^{2}HCl Spin−Echo ($\tau/2-\pi-\tau/2$) intensities in Figure 8

data set	A	J_{CO}/Hz	T_{2a}'/ms	p^a	J_{OO}/Hz	T_{2b}'/ms	$[\varepsilon^2]^b$
S_{HET} O1 (C=O)^c	1.04 ± 0.01	24.8 ± 0.2	36.0 ± 0.9				0.004
S_{HET} O2 (O^2H)^c	0.94 ± 0.02	25.6 ± 0.3	23.7 ± 0.8				0.007
S_{HET} O1 (C=O)^{d,e}	1.02 ± 0.02	24.8 ± 0.2	43.8 ± 4.1	0.53 ± 0.66	5.5 ± 4.9	43.8^f ± 4.1	0.002
S_{HET} O2 (O^2H)^{d,e}	0.99 ± 0.02	25.3 ± 0.3	31.8 ± 3.7	0.79 ± 0.06	4.5 ± 0.9	1.7 ± 2	0.001
S_Q O1 (C=O)^g	1.00 ± 0.02	24.7 ± 0.2	279^h ± 70				0.046
S_Q O2 (O^2H)^g	1.01 ± 0.02	25.3 ± 0.3	231^h ± 80				0.049

^{a} The proportion of ^{17}O nuclei with an intramolecular $^2J_{OO}$ coupling,, i.e., corresponding to the proportion of ^{17}O-labeled nuclei. ^{b} $\varepsilon^2 = \sum[I_{fit}(n) - I_{exp}(n)]^2/\sum I_{exp}(n)^2$. ^{c} Fit of the $^{17}O/^{13}C$ heteronuclear spin−echo data to eq 13. ^{d} Fit of the $^{17}O/^{13}C$ heteronuclear spin−echo data to eq 14. ^{e} One or more correlation coefficients are greater than 0.7 (see Supporting Information). ^{f} T_{2a}' was set equal to T_{2b}' (otherwise correlation coefficients of greater than 0.99 were obtained). ^{g} Fit of $S_Q(\tau) = S_{HET}(\tau)/S_{HOM}(\tau)$ to eq 15. ^{h} $1/\Delta T_2' = (1/T_{2\ HET}') - (1/T_{2\ HOM}')$.

6.1. Homonuclear ^{17}O Spin−Echo: Glycine·^{2}HCl. Experimental ^{17}O homonuclear spin−echo ($\tau/2-\pi-\tau/2$) intensities—acquired using the pulse sequence in Figure 1d (without the π pulse on the nonobserve channel)—as a function of τ for the resolved C=O and C−O^2H ^{17}O sites of glycine·^{2}HCl are shown in Figure 7. A faster dephasing is evident for the C−O^2H ^{17}O

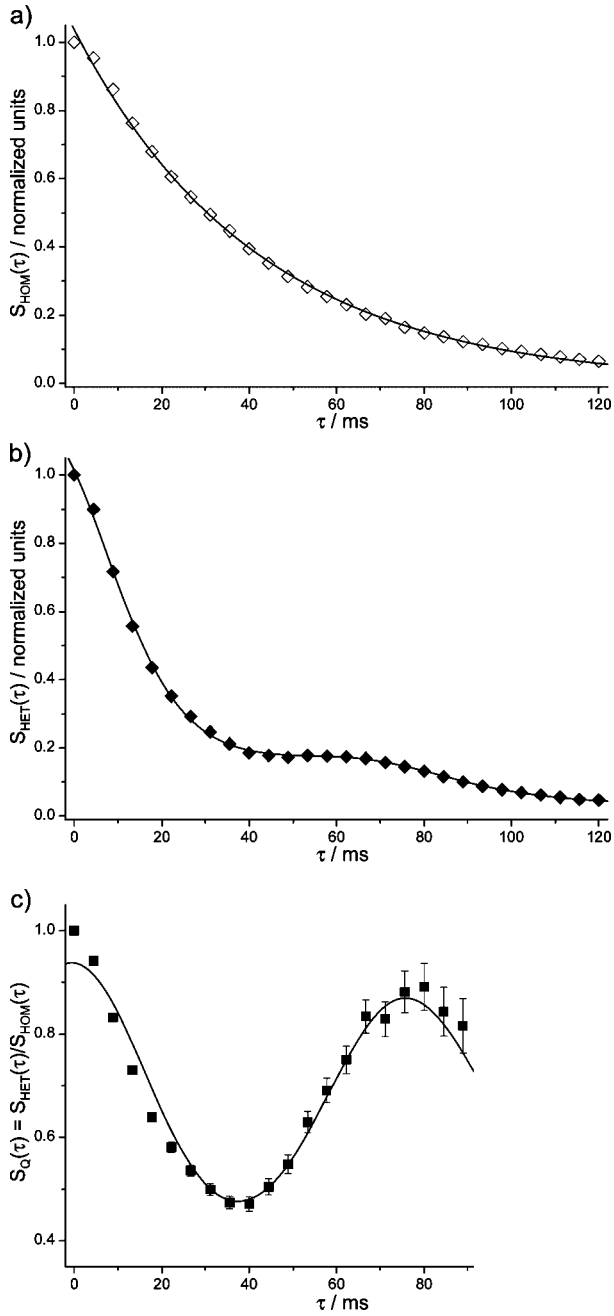

Figure 9. (a) ^{13}C homonuclear and (b) $^{13}C/^{17}O$ heteronuclear spin−echo ($\tau/2-\pi-\tau/2$) intensities for the carbonyl ^{13}C resonance in [$^2H(NH_3)$,1-^{13}C,^{15}N,$^{17}O_2$]glycine·^{2}HCl as a function of the evolution time together with best fits to eqs 11 and 17, respectively (solid lines, see Table 7). Experiments were carried out at 14.1 T ($\nu_0(^1H)$ = 600 MHz) and a MAS frequency of 22.5 kHz. The error bars for the experimental intensities were determined to be ±0.002 and are omitted for clarity. (c) The quotient $S_Q(\tau) = S_{HET}(\tau)/S_{HOM}(\tau)$ for the carbonyl ^{13}C resonance in [$^2H(NH_3)$,1-^{13}C,^{15}N,$^{17}O_2$]glycine·^{2}HCl together with the best fit to eq 18 (solid line, see Table 7). $S_Q(\tau)$ has been normalized such that $S_Q(\tau = 0) = 1.00$: experimentally, the ratio of the integrated intensities $S_{HET}(\tau = 0)/S_{HOM}(\tau = 0)$ equaled 1.01.

site. The top row (Figure 7a,b) shows fits (solid lines, see Table 5) to a decaying exponential:

$$S(\tau) = A \exp(-\tau/T_{2a}') \tag{11}$$

where A is a normalization constant and T_{2a}' is the "refocusable" transverse dephasing time.[98] While the fits in Figure 7a,b are good, a small systematic deviation of the data points from the decaying exponential is observed, which suggests the presence of an additional modulation. A CASTEP[46] calculation (see section 2.3 and Supporting Information) predicts a 7.9 Hz $^{17}O-^{17}O$ two-bond intramolecular $^2J_{OO}$ coupling for glycine·^{2}HCl. It must be remembered, however, that ^{17}O labeling is not complete; i.e., the sample contains molecules with none, one, or both of the oxygen sites ^{17}O labeled. Therefore, for a specific resonance (i.e., O1 or O2), there are separate contributions from ^{17}O nuclei with and without an intramolecular $^2J_{OO}$ coupling. As shown in Figure 7c,d, better fits (solid lines, reduced ε^2 in Table 5) are obtained with the following function that takes into account such separate contributions from ^{17}O nuclei with and without an intramolecular $^2J_{OO}$ coupling:

$$S(\tau) = A[p \cos(\pi J\tau) \exp(-\tau/T_{2a}') + (1-p) \exp(-\tau/T_{2b}')] \tag{12}$$

A discussion of the comparison of the extracted J couplings to those determined by the CASTEP calculation will be given in the following section.

6.2. Heteronuclear $^{17}O/^{13}C$ Spin−Echo: Glycine·^{2}HCl. Experimental $^{17}O/^{13}C$ heteronuclear spin−echo ($\tau/2-\pi-\tau/2$) intensities—acquired using the pulse sequence in Figure 1d—as a function of τ for the resolved C═O and C−O^{2}H ^{17}O sites of glycine·^{2}HCl are shown in Figure 8a,b. In both cases, clear J modulations are observed, and good fits (solid black lines, see Table 6) are obtained using eq 13.

$$S(\tau) = A\cos(\pi J\tau)\exp(-\tau/T_{2a}') \tag{13}$$

Note that the dephasing times for the O^{2}H ^{17}O resonance, 27 ± 1 ms for the ^{17}O homonuclear and 24 ± 1 ms for the $^{17}O/^{13}C$ heteronuclear experiment, are slightly longer than that determined for ^{13}CH-labeled L-alanine using XiX ^{1}H decoupling[103] (ν_1 = 100 kHz) at 30 kHz MAS and 600 MHz (T_2' = 20 ± 2 ms).[104]

As was the case for the ^{17}O homonuclear spin−echo data in Figure 7, slightly improved fits (see Figure 8c,d and Table 6) are obtained by considering the proportion of ^{17}O nuclei with and without an intramolecular $^2J_{OO}$ coupling ($J_1 = {}^1J_{CO}$, $J_2 = {}^2J_{OO}$):

$$S(\tau) = A \cos(\pi J_1\tau)[p \cos(\pi J_2\tau) \exp(-\tau/T_{2a}') + (1-p) \exp(-\tau/T_{2b}')] \tag{14}$$

Tables 5 and 6 present four fits (correlation coefficients are given in the Supporting Information) that depend on the proportion of ^{17}O nuclei, p, and the intramolecular $^2J_{OO}$ coupling. The correlation coefficients involving p are lowest—specifically, the biggest correlation coefficient is that between p and T_{2b}' (0.27)—for the fit of $S_{HET}(\tau)$ for O2 (O^{2}H) to eq 14, where the proportion of ^{17}O nuclei is determined as 0.79 ± 0.06 (Table 6). In this context, it is to be noted that the sample was prepared using [70%-^{17}O]H$_2$O. Considering $^2J_{OO}$, the lowest correlation coefficients are found for the fit of $S_{HOM}(\tau)$ for O1 (C═O) to eq 12 (J, p = −0.37 and J, T_{2a}' = 0.67), where $^2J_{OO}$ is determined as 8.8 ± 0.9 Hz. This is in good agreement with that predicted by the CASTEP[46] calculation (7.9 Hz) (see section 2.3 and Supporting Information).

Figure 8e,f shows the quotient $S_Q(\tau) = S_{HET}(\tau)/S_{HOM}(\tau)$, where $S_{HET}(\tau)$ and $S_{HOM}(\tau)$ refer to the $^{17}O/^{13}C$ heteronuclear and ^{17}O homonuclear spin−echo data presented in Figure 8a,b and Figure 7, respectively. $S_Q(\tau)$ is given as

$$S_Q(\tau) = A \cos(\pi J\tau) \exp(-\tau/\Delta T_2') \tag{15}$$

where

$$1/\Delta T_2' = (1/T_{2\,HET}') - (1/\Delta T_{2\,HOM}') \tag{16}$$

Table 7. Parameters Extracted from the Fits of the ^{13}C and $^{13}C-^{17}O$ Glycine·^{2}HCl Spin−Echo ($\tau/2-\pi-\tau/2$) Intensities in Figure 9

data set	A	T_{2a}'/ms	p^a	$J_1{}^b$/Hz	T_{2b}'/ms	$[\varepsilon^2]^c$
$S_{HOM}{}^d$	1.04 ± 0.03	41.8 ± 1.9				0.0005
$S_{HET}{}^{e,f}$	1.01 ± 0.004	47.4 ± 0.6	0.23 ± 0.01	25.4 ± 2.7	26.7 ± 0.7	0.0004
$S_Q{}^{f,g}$	0.94 ± 0.04	262[h] ± 149	0.15 ± 0.02	26.2 ± 0.6		0.0015

[a] The proportion of ^{17}O-labeled nuclei. [b] J_1 was set equal to J_2 (otherwise correlation coefficients of greater than 0.99 were obtained). [c] $\varepsilon^2 = \sum[I_{fit}(n) - I_{exp}(n)]^2/\sum I_{exp}(n)^2$. [d] Fit to eq 11. [e] Fit to eq 17. [f] One or more correlation coefficients are greater than 0.7 (see Supporting Information). [g] Fit of $S_Q(\tau) = S_{HET}(\tau)/S_{HOM}(\tau)$ to eq 18. [h] $1/\Delta T_2' = (1/T_{2\ HET}') - (1/T_{2\ HOM}')$.

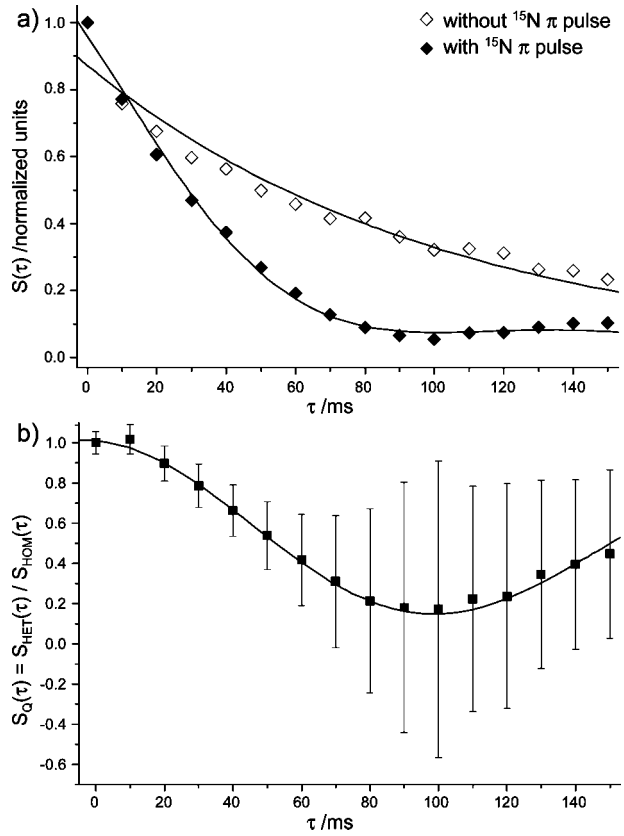

Figure 10. (a) ^{17}O homonuclear (open diamonds) and $^{17}O/^{15}N$ heteronuclear (filled diamonds) spin−echo ($\tau/2-\pi-\tau/2$) intensities for [$^{15}N_2$,$^{17}O_2$]uracil as a function of the evolution time together with best fits to eqs 11 and 19, respectively (solid lines, see Table 8). Experiments were carried out at 14.1 T ($\nu_0(^1H)$ = 600 MHz) and a MAS frequency of 20.0 kHz. The error bars for the experimental intensities were determined to be ±0.04 and are omitted for clarity. (b) The quotient $S_Q(\tau) = S_{HET}(\tau)/S_{HOM}(\tau)$ for [$^{15}N_2$,$^{17}O_2$]uracil together with the best fit to eq 20 (solid line, see Table 8). $S_Q(\tau)$ has been normalized such that $S_Q(\tau = 0) = 1.00$. Experimentally the ratio of the integrated intensities $S_{HET}(\tau = 0)/S_{HOM}(\tau = 0)$ equaled 1.02.

Good fits (see Table 6) to eq 15 are observed in Figure 8e,f, with close agreement between the fitted J couplings of 24.7 ± 0.2 and 25.3 ± 0.3 Hz (the correlation coefficients involving J are less than 0.1) and those calculated using CASTEP[46] (see section 2.3 and Supporting Information), $^1J_{CO}$ = 24.9 and 27.5 Hz for the C═O and C-OH moieties, respectively. The large fitted values for $\Delta T_2'$ (279 and 231 ms) correspond to only a slight damping by the decaying exponential term and are consistent with the dephasing times obtained from fits of the heteronuclear spin−echo data to eq 13 (see Table 6) being only slightly shorter than those obtained from fits of the homonuclear spin−echo data to eq 11 (see Table 5): 36 cf. 39 ms (C═O) and 24 cf. 27 ms (O^2H).

6.3. Homonuclear ^{13}C and Heteronuclear $^{13}C/^{17}O$ Spin−Echo: Glycine·^{2}HCl. ^{13}C homonuclear and $^{13}C/^{17}O$ heteronuclear spin−echo ($\tau/2-\pi-\tau/2$) intensities as a function of τ for glycine·^{2}HCl (^{13}C labeled only at the carboxylic acid carbon)

Table 8. Parameters Extracted from the Fits of the ^{17}O and $^{17}O-^{15}N$ Uracil Spin−Echo ($\tau/2-\pi-\tau/2$) Intensities in Figure 10

data set	A	T_{2a}'/ms	p^a	$^{2h}J_{NO}{}^b$/Hz	$[\varepsilon^2]^c$
$S_{HOM}{}^{d,e}$	0.87 ± 0.03	102 ± 7			0.0075
$S_{HET}{}^{e,f}$	0.96 ± 0.04	62[g] ± 10	0.66 ± 0.14	5.8 ± 0.6	0.0026
$S_Q{}^{e,h}$	1.01 ± 0.05	550[i] ± 1479	0.85 ± 0.20	5.1 ± 0.6	0.0019

[a] The relative contribution of O4 ^{17}O nuclei to the ^{17}O resonance (overlapping O2 and O4). [b] J_1 was set equal to J_2 (otherwise correlation coefficients of greater than 0.99 were obtained). [c] $\varepsilon^2 = \sum[I_{fit}(n) - I_{exp}(n)]^2/\sum I_{exp}(n)^2$. [d] Fit to eq 11. [e] One or more correlation coefficients are greater than 0.7 (see Supporting Information). [f] Fit to eq 19. [g] $T'_{2a}$was set equal to T'_{2b}(otherwise correlation coefficients of greater than 0.99 were obtained). [h] Fit of $S_Q(\tau) = S_{HET}(\tau)/S_{HOM}(\tau)$ to eq 20. [i] $1/\Delta T_2' = (1/T_{2\ HET}') - (1/T_{2\ HOM}')$.

acquired using the pulse sequence in Figure 1e (without and with the ^{17}O π pulse) are shown in Figure 9a,b, respectively. The ^{13}C homonuclear spin−echo data (Figure 9a) are well fit (see Table 7) to the simple decaying exponential function of eq 11.

Unlike for the $^{17}O/^{13}C$ heteronuclear spin−echo data in Figure 8a,b, zero-crossings are not observed for the $^{13}C/^{17}O$ heteronuclear spin−echo data (see Figure 9b). In this context, the partial ^{17}O enrichment of the oxygen sites must be remembered, with there being a proportion $(1 - p)^2$ of the ^{13}C nuclei having no one-bond J coupling to ^{17}O—a situation similar to the ^{13}C spin−echo data presented in ref 105 for a partially enriched cellulose sample. The experimental data were fit (solid line in Figure 9b) using the function

$$S(\tau) = A[\exp(-\tau/T_{2a}')\{p^2\cos(\pi J_1\tau)\cos(\pi J_2\tau) + p(1-p)\cos(\pi J_1\tau) + p(1-p)\cos(\pi J_2\tau)\} + \exp(-\tau/T_{2b}')(1-p)^2] \quad (17)$$

where p is the probability that one oxygen site is ^{17}O labeled (this is assumed to be the same for the two oxygen sites), and separate dephasing times are considered for ^{13}C with and without a ^{17}O neighbor(s). A good fit (setting $J_1 = J_2$) of the experimental data to eq 17 is evident from Figure 9b; however, high correlation coefficients involving J (J, $p = -0.65$; J, $T_{2a}' = -0.61$; J, $T_{2b}' = 0.40$) and p (p, $J = -0.65$; p, $T_{2a}' = 0.87$; p, $T_{2b}' = -0.66$) are observed.

Figure 9c shows the quotient $S_Q(\tau) = S_{HET}(\tau)/S_{HOM}(\tau)$, where $S_{HET}(\tau)$ and $S_{HOM}(\tau)$ refer to the $^{13}C/^{17}O$ heteronuclear and ^{13}C homonuclear spin−echo data presented in Figure 9a,b. $S_Q(\tau)$ is given as

$$S_Q(\tau) = A\{\exp(-\tau/\Delta T_2')[p^2\cos(\pi J_1\tau)\cos(\pi J_2\tau) + p(1-p)\cos(\pi J_1\tau) + p(1-p)\cos(\pi J_2\tau)] + (1-p)^2\} \quad (18)$$

Note that the decaying exponential term corresponding to the difference ($\Delta T_2'$ is defined in eq 16) between the dephasing times for the heteronuclear and homonuclear spin−echo is omitted for the proportion of ^{13}C without a directly bonded ^{17}O nucleus because the ^{17}O π pulse is not expected to change the dephasing time for this proportion of ^{13}C without a directly

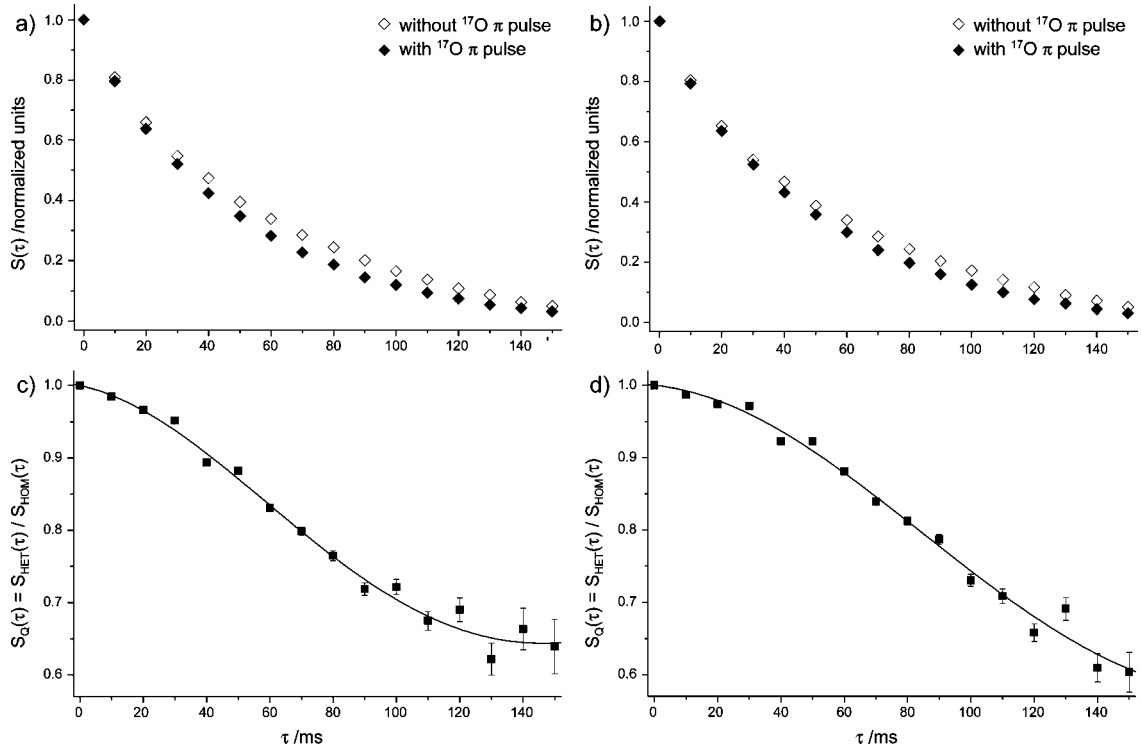

Figure 11. (a,b) ^{15}N homonuclear (open diamonds) and ^{15}N/^{17}O heteronuclear (filled diamonds) spin−echo ($\tau/2-\pi-\tau/2$) intensities for the (a) N1 and (b) N3 resonances of [$^{15}N_2$,$^{17}O_2$]uracil as a function of the evolution time. Experiments were carried out at 14.1 T ($\nu_0(^1H) = 600$ MHz) and a MAS frequency of 20.0 kHz. The error bars for the experimental intensities were determined to be ±0.0008 and are omitted for clarity. (c,d) The quotient $S_Q(\tau) = S_{HET}(\tau)/S_{HOM}(\tau)$ for the (c) N1 and (d) N3 resonances of [$^{15}N_2$,$^{17}O_2$]uracil together with the best fits (solid line, see Table 9) to eq 21. $S_Q(\tau)$ has been normalized such that $S_Q(\tau = 0) = 1.00$. Experimentally the ratio of the integrated intensities $S_{HET}(\tau = 0)/S_{HOM}(\tau = 0)$ equaled 1.001 and 0.999 for the (c) N1 and (d) N3 resonances, respectively.

Table 9. Parameters Extracted from the Fits of the ^{15}N and ^{15}N−^{17}O Uracil Spin−Echo ($\tau/2-\pi-\tau/2$) Data in Figures 11 and 12

data set	A	p^a	J_{NO}/Hz	J_{NN}/Hz	T_{2a}'/ms	T_{2b}'/ms	$[\varepsilon^2]^b$
S_Q N1−O4[c,d]	1.00 ± 0.01	0.22 ± 0.01	6.7 ± 0.4		294[e] ± 38		0.0003
S_Q N3−O4[c,d]	1.00 ± 0.01	0.27 ± 0.03	4.8 ± 0.5		585[e] ± 98		0.0003
S_{HET} N1−O4[d,f]	0.93 ± 0.01	0.51 ± 0.15	0.0 ± 67	2.7 ± 0.1	121 ± 4	33.7 ± 4.6	0.0005
S_{HET} N3−O4[d,f]	0.94 ± 0.01	0.69 ± 0.07	0.0 ± 1775	2.6 ± 0.1	110 ± 2	25.4 ± 3.1	0.0003

[a] The proportion of ^{15}N nuclei with a J coupling to an ^{17}O nucleus, corresponding to the degree of ^{17}O labeling at the O4 site. [b] $\varepsilon^2 = \sum[I_{fit}(n) - I_{exp}(n)]^2/\sum I_{exp}(n)^2$. [c] Fit of $S_Q(\tau) = S_{HET}(\tau)/S_{HOM}(\tau)$ to eq 21; J corresponds to $^{2h}J_{N,O}$. [d] One or more correlation coefficients are greater than 0.7 (see Supporting Information). [e] $1/\Delta T_2' = (1/T_{2\ HET}') - (1/T_{2\ HOM}')$. [f] Fit to eq 14.

bonded ^{17}O nucleus. A good fit (setting $J_1 = J_2$, see Table 7) to eq 18 is observed in Figure 9c. The correlation coefficients involving J are small (magnitude 0.04−0.12) for the fit of the $S_Q(\tau)$ data—this is in contrast to the fit of the heteronuclear spin−echo data in Figure 9b—and close agreement between the fitted J coupling (26.7 ± 0.6 Hz) and the average of those determined by CASTEP ($^1J_{CO} = 24.9$ and 27.5 Hz for the C═O and C−OH moieties, respectively) is observed. In contrast, high correlation coefficients involving p (p, $\Delta T_2' = -0.76$; p, $A = 0.93$) mean that the degree of ^{17}O labeling cannot be reliably determined from this fit.

6.4. Homonuclear ^{17}O and Heteronuclear ^{17}O/^{15}N Spin−Echo: Uracil. In the uracil molecule, there are two distinct nitrogen and oxygen sites, with the crystal structure (Figure 2b) of uracil revealing that only one of the two distinct oxygen atoms participates in NH···O hydrogen-bonding: oxygen O4 forms two intermolecular NH···O hydrogen bonds to N1 and N3. In the ^{17}O MAS spectrum of [$^{15}N_2$,$^{17}O_2$]uracil shown in Figure 3b, the second-order quadrupolar broadened line shapes for the two distinct ^{17}O resonances are unresolved from each other. In a spin−echo analysis, it is thus necessary to consider the contribution from ^{17}O nuclei with and without hydrogen-bond-mediated J couplings to N1 and N3.

Figure 10a compares homonuclear ^{17}O (open diamonds) and heteronuclear ^{17}O/^{15}N (filled diamonds) spin−echo ($\tau/2-\pi-\tau/2$) data obtained using the pulse sequence in Figure 1d (without and with the ^{15}N π pulse). Best fits (see Table 8) are shown as solid lines for the homonuclear spin−echo data fit to the simple decaying exponential function of eq 11 and the heteronuclear spin−echo data (for J_1 set equal to J_2 and T_{2a}' set equal to T_{2b}') fit to

$$S(\tau) = A[p\cos(\pi J_1\tau)\cos(\pi J_2\tau)\exp(-\tau/T_{2a}') + (1-p)\exp(-\tau/T_{2b}')] \quad (19)$$

Figure 10b shows the quotient $S_Q(\tau) = S_{HET}(\tau)/S_{HOM}(\tau)$, where $S_{HET}(\tau)$ and $S_{HOM}(\tau)$ refer to the ^{17}O/^{15}N heteronuclear and ^{17}O homonuclear spin−echo data presented in Figure 10a. $S_Q(\tau)$ is given as

$$S_Q(\tau) = A\{p\cos(\pi J_1\tau)\cos(\pi J_2\tau)\exp(-\tau/\Delta T_2') + (1-p)\} \quad (20)$$

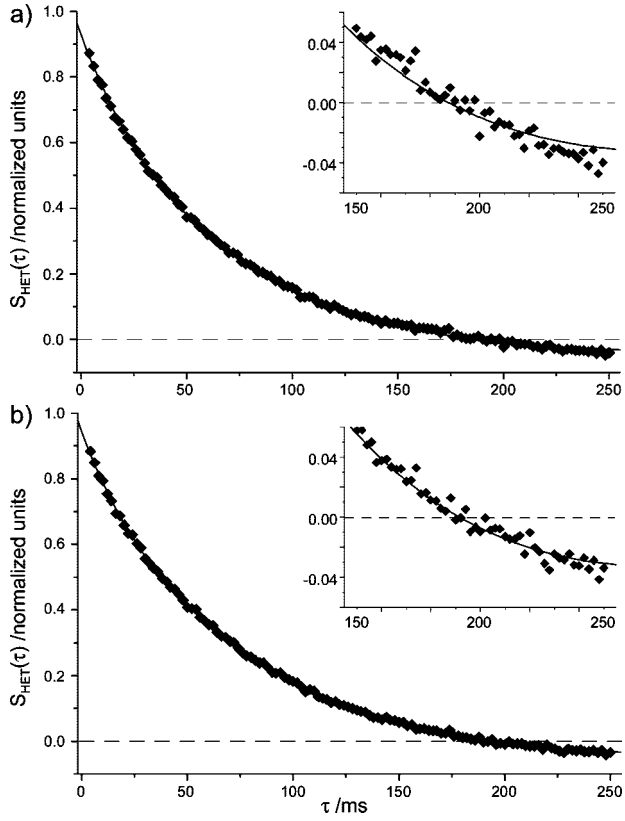

Figure 12. $^{15}N/^{17}O$ heteronuclear spin−echo ($\tau/2-\pi-\tau/2$) intensities for the (a) N1 and (b) N3 ^{15}N sites of [$^{15}N_2$,$^{17}O_2$]uracil as a function of the evolution time together with the best fits (black curves) to eq 14 (see Table 9). The error bars for the experimental ^{15}N data points of both sites were determined to be ±0.003 and are omitted for clarity (16 transients were coadded for each τ increment). Expansions for $\tau = 160-250$ ms are shown as insets. Experiments were carried out at 14.1 T ($\nu_0(^1H) =$ 600 MHz) and a MAS frequency of 20.0 kHz.

A good fit (for J_1 set equal to J_2, see Table 8) to eq 20 is observed in Figure 10b. The $^{2h}J_{NO}$ couplings as determined from the fits of $S_{HET}(\tau)$ and $S_Q(\tau)$, namely 5.8 ± 0.6 and 5.1 ± 0.6 Hz, respectively, are in agreement with each other. Smaller correlation coefficients involving J are found for the fit of $S_Q(\tau)$, although those for $S_{HET}(\tau)$ are still reasonable (J, $p = 0.52$; J, $T_{2a}' = -0.41$; J, $A = 0.37$ for $S_{HET}(\tau)$; and J, $p = -0.25$; J, $\Delta T_2' = -0.01$; J, $A = 0.15$ for $S_Q(\tau)$). The experimental average $^{2h}J_{NO}$ couplings are in good agreement with those determined by a CASTEP[46] calculation (see section 2.3 and Supporting Information), namely $^{2h}J_{N1,O4} = 6.1$ and $^{2h}J_{N3,O4} = 4.6$ Hz. As shown in the Supporting Information, all other $^{15}N-^{17}O$ J couplings (both inter- and intramolecular) are calculated to be of magnitude 0.5 Hz or less. Note that CASTEP calculations have recently been shown to provide excellent accuracy for hydrogen-bond-mediated $^{2h}J_{NN}$ couplings[106] determined experimentally using ^{15}N spin−echo MAS experiments.[40,107]

6.5. Homonuclear ^{15}N and Heteronuclear $^{15}N/^{17}O$ Spin−Echo: Uracil. Figure 11a,b compares homonuclear ^{15}N (open diamonds) and heteronuclear $^{15}N/^{17}O$ (filled diamonds) spin−echo ($\tau/2-\pi-\tau/2$) data obtained using the pulse sequence in Figure 1e (without and with the ^{17}O π pulse) for the N1 and N3 resonances. In both cases, there is a small yet significant difference between the homonuclear and heteronuclear spin−echo data. Figure 11c,d shows the quotient $S_Q(\tau) = S_{HET}(\tau)/S_{HOM}(\tau)$ for the N1 and N3 resonances, where $S_{HET}(\tau)$ and $S_{HOM}(\tau)$ refer to the $^{15}N/^{17}O$ heteronuclear and ^{15}N homonuclear spin−echo data presented in Figure 11a,b. $S_Q(\tau)$ is given as

$$S_Q(\tau) = A\{p\cos(\pi J\tau)\exp(-\tau/\Delta T_2') + (1-p)\} \qquad (21)$$

where p corresponds to the proportion of ^{15}N nuclei with a J coupling to an ^{17}O nucleus. Good fits (see Table 9) to eq 21 are observed in Figure 11c,d. Although there is a very high correlation between p and J (the p, J correlation coefficient equals −0.98 and −0.99 for N1 and N3, respectively), the fitted J couplings of 6.7 ± 0.4 Hz (N1) and 4.8 ± 0.5 Hz (N3) are in remarkably good agreement with those determined by the CASTEP[46] calculation, namely $^{2h}J_{N1,O4} = 6.1$ and $^{2h}J_{N3,O4} = 4.6$ Hz.

Figure 12 presents $^{15}N/^{17}O$ heteronuclear spin−echo ($\tau/2-\pi-\tau/2$) data for the N1 and N3 uracil resonances for a spin−echo duration up to 250 ms (obtained experimentally separately from the data presented in Figure 11). The CASTEP[46] calculation (see section 2.3 and Supporting Information) predicts an intramolecular J_{NN} coupling in uracil, $^2J_{N1,N3} = 2.7$ Hz. This is consistent with the observation of zero-crossings at long spin−echo durations (~200 ms) and the good fits (see Table 9) to eq 14 (where $J_1 = {}^2J_{NN}$, $J_2 = {}^{2h}J_{NO}$). Specifically, the correlation coefficients involving $^2J_{NN}$ are reasonable (maximum magnitude 0.59 and 0.62 for the N1 and N3 data, respectively), and the experimental values of $^2J_{NN} = 2.7 \pm 0.1$ and 2.6 ± 0.1 Hz are in perfect agreement with the calculated value of $^2J_{N1,N3} = 2.7$ Hz. Table 9 shows that it is, however, not possible to determine $^{2h}J_{NO}$ from the fit to the heteronuclear spin−echo data. In this respect, note that the modulation under the homonuclear $^2J_{N1,N3}$ coupling will be present for both the ^{15}N homonuclear and $^{15}N/^{17}O$ heteronuclear spin−echo experiments. It is removed by taking the quotient $S_Q(\tau) = S_{HET}(\tau)/S_{HOM}(\tau)$, hence allowing the observation in Figure 11c,d of the modulation due to the proportion of ^{15}N with a hydrogen-bond-mediated J coupling to a ^{17}O nucleus.

7. Conclusions

The feasibility of heteronuclear solid-state MAS NMR experiments for probing $^{15}N-^{17}O$ dipolar and J couplings in two isotopically labeled model compounds, glycine·^{2}HCl and uracil, has been demonstrated. Specifically, the R^3-HMQC experiment yields two-dimensional $^{15}N-^{17}O$ correlations for dipolar coupled ^{15}N and ^{17}O nuclei; for glycine·^{2}HCl, the intensity of the resolved peaks for the C=O and O^{2}H ^{17}O resonances corresponds to the relative magnitude of the respective $^{15}N-^{17}O$ dipolar couplings. Fits of the initial buildup ($\Delta S/S < 0.2$) in $^{17}O-^{15}N$ REDOR curves for glycine·^{2}HCl yield effective dipolar couplings in agreement with (±20%) the root-sum-squared dipolar couplings[49] determined from the crystal structure. Experimental $^{15}N-^{17}O$ REAPDOR curves for the ^{15}N resonance in glycine·^{2}HCl and the two distinct ^{15}N resonances in uracil are well fit to the universal curve presented by Goldbourt et al.[34]

The first (to the best of our knowledge) solid-state NMR determination of $^{13}C-^{17}O$, $^{17}O-^{17}O$, and $^{15}N-^{17}O$ J couplings is reported. Heteronuclear $^{13}C-^{17}O$ and $^{15}N-^{17}O$ J couplings are experimentally determined from fits of the quotient of the integrated intensity obtained in a heteronuclear and a homonuclear spin−echo experiment, $S_Q(\tau) = S_{HET}(\tau)/S_{HOM}(\tau)$. Importantly, for $S_Q(\tau)$, there is only a small damping of the signal

(105) Brown, S. P.; Emsley, L. *J. Magn. Reson.* **2004**, *171*, 43.
(106) Joyce, S. A.; Yates, J. R.; Pickard, C. J.; Brown, S. P. *J. Am. Chem. Soc.* **2008**, *130*, 12663.
(107) Brown, S. P.; Perez-Torralba, M.; Sanz, D.; Claramunt, R. M.; Emsley, L. *Chem. Commun.* **2002**, 1852.

that is fit to a decaying exponential corresponding to the *difference* in the dephasing times for the heteronuclear and homonuclear spin−echo experiments. Excellent agreement is observed between the experimentally determined J couplings and those calculated using the first-principles CASTEP code.[46]

To the best of our knowledge, this is the first demonstration of $^{15}N-^{17}O$ solid-state NMR experiments. ^{17}O solid-state NMR is being increasingly employed as a probe of biological molecules.[6,24,25,52,108−110] Given the importance of NH···O hydrogen-bonding, e.g., in proteins and nucleic acids, there is evidently much potential to further apply the $^{15}N-^{17}O$ solid-state NMR experiments demonstrated in this paper, so as to unambiguously identify specific structure-determining hydrogen-bonding interactions.

Acknowledgment. Funding from the EPSRC, BBSRC, and the Leverhulme Trust is acknowledged. Computational work was carried out at the Centre for Scientific Computing at the University of Warwick (SRIF funded) and the EaStCHEM Research Computing Facility at the University of St. Andrews. We thank Paul Hodgkinson (Durham) for making available his MATLAB fitting routines.

Supporting Information Available: Correlation coefficients for fits of spin−echo data, spin−echo spectra obtained for $\tau = 0$, full listing of calculated J couplings, complete ref 45, and geometrically optimized (CASTEP) crystal structures, as used for the calculation of the NMR J couplings. This material is available free of charge via the Internet at http://pubs.acs.org.

JA805898D

(108) Wong, A.; Howes, A. P.; Pike, K. J.; Lemaitre, V.; Watts, A.; Anupold, T.; Past, J.; Samoson, A.; Dupree, R.; Smith, M. E. *J. Am. Chem. Soc.* **2006**, *128*, 7744.
(109) Lemaitre, V.; de Planque, M. R. R.; Howes, A. P.; Smith, M. E.; Dupree, R.; Watts, A. *J. Am. Chem. Soc.* **2004**, *126*, 15320.
(110) Kwan, I. C. M.; Mo, X.; Wu, G. *J. Am. Chem. Soc.* **2007**, *129*, 2398.